JGR Solid Earth

RESEARCH ARTICLE
10.1029/2020JB020242

A Systematic Approach to Mapping Regimes of Earthquake-Induced Static Stress Changes Acting on Magmatic Pathways

A. P. Jenkins[1], J. Biggs[1], A. C. Rust[1], and R. L. Jara[2]

[1]School of Earth Sciences, University of Bristol, Bristol, UK, [2]BHP Exploration, Lima, Perú

Key Points:

- We map seven normal stress change regimes (>1 kPa) on three perpendicular magma pathways after subduction thrust earthquakes
- Slip magnitude, distribution, and dip control regime distribution, with hotter, mature arcs more sensitive to stress changes
- We show how rapid stress field variations caused by earthquakes could affect patterns of magma ascent and storage

Supporting Information:

- Supporting Information S1

Correspondence to:

A. P. Jenkins,
alexander.jenkins@bristol.ac.uk

Citation:

Jenkins, A. P., Biggs, J., Rust, A. C., & Jara, R. L. (2021). A systematic approach to mapping regimes of earthquake-induced static stress changes acting on magmatic pathways. *Journal of Geophysical Research: Solid Earth*, *126*, e2020JB020242. https://doi.org/10.1029/2020JB020242

Received 29 MAY 2020
Accepted 5 DEC 2020

Abstract Large earthquakes alter the crustal stress field across great distances (hundreds to thousands of kilometers) over geologically short timescales (seconds to years). These stress changes can affect magmatic systems, triggering (or suppressing) volcanic unrest and eruption, along with other deeper processes. We use simple kinematic source models in an isotropic elastic half-space to assess earthquake-induced static stress changes (>1 kPa) over the entire thickness of the lithosphere and consider the implications for magma ascent and storage. Modeling subduction zone earthquakes, we calculate static normal stress changes with depth on three mutually perpendicular end-member magma pathways: vertical arc-parallel, vertical arc-perpendicular, and horizontal. From this, we define seven stress change regimes within the adjacent volcanic arc. Three of these regimes may strongly encourage magma ascent in dykes by inducing unclamping (decreased compressive normal stress) of vertical pathways which increases in magnitude toward the surface and clamping of horizontal pathways. Two of the regimes may encourage stalling and storage of magma in sills near the base of the crust by inducing unclamping of horizontal pathways at depth. The spatial distribution of the regimes is largely dependent on earthquake magnitude, but also varies with slip distribution and interface dip. We show how the responses of magmatic systems to earthquakes also depends on the stress change magnitude and the state of the magmatic system, with a greater impact expected for larger stress changes acting on weaker, more thermally mature systems.

1. Introduction

1.1. The Crustal Stress Field

Rapid magma transfer through the Earth's crust occurs by flow in self-propagating sheet intrusions such as dykes (Clemens & Mawer, 1992; Petford et al., 1993, 2000; Rubin, 1995; Ruprecht & Plank, 2013). Magmatic intrusions are generally mode I fractures and so preferentially open parallel to the minimum principal stress direction (σ_3), although they may be influenced by structures or weaknesses in the host rock such as faults, fractures, or layering (Anderson, 1951; Drymoni et al., 2020; Gudmundsson, 2002, 2020; Magee et al., 2013; Nakamura, 1977; Rivalta et al., 2015; Ziv et al., 2000). At the regional level, crustal stress and structure is primarily controlled by plate tectonics (Kearey et al., 2009; Zoback, 1992; Zoback et al., 1989). However, measurement of the present-day crustal stress field provides abundant evidence for spatiotemporal variations unrelated to plate motions (Heidbach et al., 2018). These variations, caused by factors such as topography, recent earthquakes, and crustal heterogeneities (e.g., layering, structure, previous magmatic activity) can have important implications for magmatic systems (e.g., Cembrano & Lara, 2009; A. Gudmundsson, 2011; Lupi et al., 2020; Maccaferri et al., 2014; Pinel & Jaupart, 2005).

We investigate the impact of large earthquakes on magmatism. Large earthquakes alter the crustal stress field over hundreds to thousands of kilometers at timescales from seconds or minutes due to the elastic response of the crust, to years or tens of years for deeper postseismic processes (Becker et al., 2018; Heidbach et al., 2018; Levandowski et al., 2018; Piersanti et al., 1995; Pollitz et al., 1998). Earthquake-driven stress changes can be substantial, such as the near-complete stress drop, or even reversal of the stress field, observed following the 2011 M_w 9.0 Tohoku megathrust earthquake (Hardebeck & Okada, 2018). Numerical models of magmatic systems generally do not consider these stress changes, often assuming a lithostatic stress state or a constant tectonic stress such as extension in rifts or compression at subduction zones (e.g., Chaussard & Amelung, 2014; Maccaferri et al., 2010; Menand et al., 2010; Roman & Heron, 2007). However,

the fast rates of magma transport (cm or m s^{-1}) relative to tectonic loading (cm yr^{-1}) may give magmatic systems some degree of independence from the tectonic setting (De Saint Blanquat et al., 2011), whereas earthquake-driven stress changes may occur over timescales more likely to influence magma transport.

Several studies have investigated the triggering of volcanic eruptions by earthquakes. Both dynamic stress changes (due to the passage of seismic waves: Hill et al., 2002; Linde & Sacks, 1998; Manga & Brodsky, 2006) and static stress changes (due to the elastic relaxation of the crust: Bonali et al., 2013, 2015; Hill et al., 2002; Nishimura, 2017; Walter & Amelung, 2007; Watt et al., 2009) have been postulated as causative mechanisms for eruption triggering. However, volcanic eruption is only one possible response of the magmatic system and changes induced by a large earthquake may not culminate in an eruption. Recent work has identified noneruptive responses to large earthquakes, including seismicity and surface deformation (De la Cruz-Reyna et al., 2010; Hill-Butler et al., 2020; Pritchard et al., 2013; Takada & Fukushima, 2013) and static stress changes have also been implicated in inhibiting eruption (Ebmeier et al., 2016). Furthermore, volcanoes represent only the upper, most easily observable parts of the magmatic system. New views on the architecture of magma reservoirs envisage a transcrustal system containing variable melt fractions, extending from the surface to the magma source in the mantle (Cashman et al., 2017; Sparks et al., 2019). Therefore, we consider the potential effects of earthquake-driven stress changes across the entire crust. While dynamic stress changes may be important, particularly in the shallow, bubble-rich parts of the system, we consider only static stress changes.

1.2. 3D Static Stress Change

We model coseismic static stress changes caused by (mega)thrust earthquakes at subduction zones and consider how they will affect magma ascent and storage in the adjacent volcanic arc. Megathrust earthquakes are the most powerful on Earth, generating the largest stress changes, and have frequently been implicated in eruption triggering (e.g., Walter & Amelung, 2007). In general, subduction interface earthquakes relax horizontal compressional stresses within the volcanic arc and so are expected to encourage magma ascent (Walter & Amelung, 2007). Although static stress changes are small ($<\approx 1$ MPa: Stein, 1999) compared to the theoretical strength of the crust ($\sigma_1 - \sigma_3 =$ 10's–100's MPa: Brace & Kohlstedt, 1980; Byerlee, 1978), evidence from earthquake aftershocks and induced seismicity shows that these small stress changes are sufficient to trigger brittle failure (Ellsworth, 2013; King et al., 1994; Stein, 1999). This leads to the contention that much of the Earth's crust is in a critically stressed state, within around one earthquake stress drop of failure (typically 3–10 MPa: Kanamori & Anderson, 1975; McGarr, 2014; Sibson, 2017; Townend & Zoback, 2000). Therefore, magmatic systems likely also exist in a critically stressed state, at least transiently, whereby small stress changes may possibly lead to observable effects such as unrest or eruption. This critically stressed state is evidenced by the high number of actively deforming volcanoes (Biggs & Pritchard, 2017), theoretical studies suggesting that only relatively small magma overpressures may be sustained before failure (A. Gudmundsson, 2012), and evidence that even tidal stresses can affect how magmatic systems deform (Scholz et al., 2019).

Previous studies investigating static stress changes on volcanic systems calculated either the mean stress change on the inferred sub-volcanic magma chamber (Hill et al., 2002; Walter & Amelung, 2007), or the normal stress change on the inferred volcanic conduit (Bonali et al., 2013). Nostro et al. (1998) considered how the shape and orientation of the magma plumbing system affects the calculated stress changes following nearby large normal faulting earthquakes. Building on these concepts, we present a method for assessing static stress changes to more fully capture their magnitude, orientation, and gradient with depth over the entire lithosphere. Modeling subduction zone earthquakes as rectangular uniform-slip dislocations in an homogenous elastic halfspace, we calculate static normal stress changes on three mutually perpendicular end-member magma pathways: vertical arc-parallel and arc-perpendicular pathways (dykes) and horizontal pathways (sills), where "arc" refers to the volcanic arc, which strikes parallel to subduction zone interface (Figure 1a). These pathways represent current or potential magma conduits, which may be influenced by existing crustal weaknesses such as faults, fractures, or layering. We use the normal stress changes on these pathways (clamping/unclamping) as a proxy for the magma response. Analyzing the normal stress changes as a function of depth, we define a set of stress change regimes produced by typical subduction interface earthquakes and map out their spatial distributions. These regimes simplify the otherwise complex stress

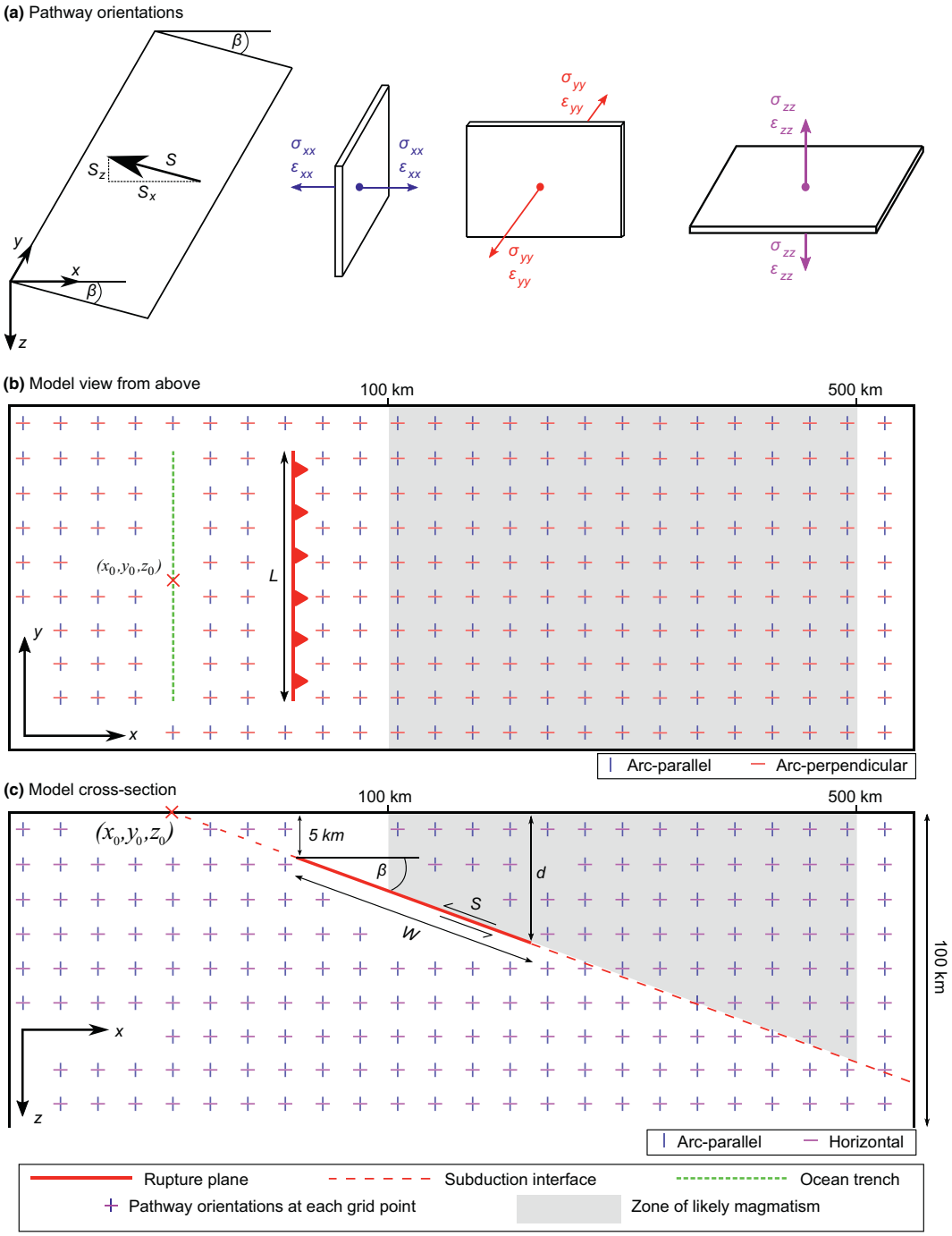

Figure 1. (a) Orientation of the subduction interface and the end-member pathways within the defined coordinate system. β is the dip of the subduction interface, S shows the slip vector, with S_x and S_z the components of slip in the x- and z-directions respectively. The end-member pathways are: arc-parallel and vertical (blue), arc-perpendicular and vertical (red), and horizontal (pink). (b) Plan and, (c) cross-section views of the idealized model. L-rupture length, W-down-dip rupture width, S- slip magnitude, d-depth to bottom of rupture. The oceanic trench marks the intercept of the subduction interface with the model surface at $z = 0$. The portrayed grid spacing is not indicative of actual model grid size.

field changes and facilitate interpretation and discussion of the potential implications for magma ascent and storage. The results presented here represent the first fully three-dimensional analysis of static stress changes from a magmatic perspective and are therefore necessarily simplified. Future work should build on this, most notably through the inclusion of layered models and explicit calculation of the magmatic response.

2. Background and Theory

2.1. Dislocation Theory

Slip during an earthquake changes the elastic strain and stress fields in the surrounding rock. We model this computationally using elastic dislocation theory, where a finite rectangular dislocation is embedded into an initially unstrained elastic halfspace. Slip across the dislocation generates a displacement field (u_{ij}) in the surrounding halfspace, the spatial derivatives of which give the elastic strain tensor field (ϵ_{ij})

$$\epsilon_{ij} = \frac{1}{2}\left(\frac{\delta u_i}{\delta x_j} + \frac{\delta u_j}{\delta x_i}\right), \tag{1}$$

where i and j correspond to the three mutually perpendicular axes x, y, and z, and contractional deformation causes negative strain. We define the y-axis as parallel to the strike of the subduction zone interface, the x-axis as horizontal and parallel to the dip direction of the subduction interface, and the z-axis as vertical (Figure 1a).

Considering a pure thrust earthquake along a shallowly dipping subduction interface, most slip will occur in the x-direction, with a small component of slip in the z-direction and no slip in the y-direction. Induced normal strains in the x-direction (ϵ_{xx}) will therefore generally be larger than normal strains in the z-direction (ϵ_{zz}), which will generally be larger than normal strains in the y-direction (ϵ_{yy}). As there is no slip in the y-direction, any displacements in the y-direction must be induced in response to displacements in the x- and z-directions.

2.2. Normal Stress Changes on End-Member Pathways

Hooke's Law in three dimensions states that the normal stress on a structure depends on both the strain normal to that structure and the volumetric strain

$$\Delta\sigma_{ij} = 2\mu\epsilon_{ij} + \lambda\epsilon_{kk}\delta_{ij}, \tag{2}$$

where σ_{ij} is the stress tensor, μ is the shear modulus, λ is Lamé's first parameter, δ_{ij} is the Kronecker delta, and ϵ_{kk} is the induced volumetric strain. The normal stress changes acting on arc-parallel ($\Delta\sigma_{xx}$), arc-perpendicular ($\Delta\sigma_{yy}$), and horizontal ($\Delta\sigma_{zz}$) pathways (Figure 1a) are therefore given by

$$\Delta\sigma_{xx} = 2\mu\epsilon_{xx} + \lambda\left(\epsilon_{xx} + \epsilon_{yy} + \epsilon_{zz}\right) \tag{3}$$

$$\Delta\sigma_{yy} = 2\mu\epsilon_{yy} + \lambda\left(\epsilon_{xx} + \epsilon_{yy} + \epsilon_{zz}\right) \tag{4}$$

$$\Delta\sigma_{zz} = 2\mu\epsilon_{zz} + \lambda\left(\epsilon_{xx} + \epsilon_{yy} + \epsilon_{zz}\right), \tag{5}$$

where $\epsilon_{xx} + \epsilon_{yy} + \epsilon_{zz}$ is the induced volumetric strain, tensile stresses are positive, and

$$\mu = \frac{E}{2(1+\nu)} \tag{6}$$

$$\lambda = \frac{E\nu}{(1+\nu)(1-2\nu)}, \tag{7}$$

where E is the Young's modulus and ν is Poisson's ratio. The mean stress change ($\Delta\sigma_{kk}$) is given by the mean of the normal stress changes on the three end-member pathways

$$\Delta\sigma_{kk} = \frac{\Delta\sigma_{xx} + \Delta\sigma_{yy} + \Delta\sigma_{zz}}{3}. \tag{8}$$

The normal stress changes on the end-member pathways (hereafter "stress changes") are not independent of one another as they all depend on the volumetric strain. The importance of the induced volumetric strain

depends on Poisson's ratio; the greater Poisson's ratio, the larger λ becomes relative to μ and therefore the volumetric strain contribution becomes larger (Figure S2).

2.3. Clamping and Unclamping of Pathways

Magma pathways exhibit many forms and geometries and can be modeled using a variety of methods (Dahm, 2000; Rivalta et al., 2015; Taisne & Jaupart, 2009). The expansion and propagation of intrusions is driven by magma overpressure (P_o), which is controlled by magma buoyancy, the host rock stress acting normal to the intrusion (σ_n), and, if the pathway is connected to the magma source, the excess pressure in the source region (P_e) (A. Gudmundsson, 2012). Earthquakes potentially alter all three of these factors, however, we model only changes to the normal stress ($\Delta\sigma_n$) on the basis that $\Delta\sigma_n$ is generally much larger than changes to magma buoyancy and P_e for the following two reasons: (1) Magma buoyancy will only change significantly if the earthquake induces volatile exsolution; (2) P_e is only a factor if the magma pathway is connected to the magma source region, in which case the source region will likely be located deeper and further from the earthquake and so will experience smaller stress changes. Furthermore, any stress changes acting on the magma source region will be opposed by changes to the internal magma pressure governed by the magma compressibility, suppressing changes to P_e (Albino et al., 2010). We therefore, make the simplifying assumption that changes to the magma overpressure caused by an earthquake (ΔP_o) depend only on $\Delta\sigma_n$.

At the walls of an intrusion, the overpressure, P_o, acts outwards against σ_n in the host rock. We use the term "clamping" (e.g., Bonini, 2019; Bonali et al., 2015; Freed, 2005) to refer to an increase in the compressive normal stress on a pathway caused by an earthquake ($\Delta\sigma_n$ is negative for clamping as tensile stresses are positive). For a magmatic pathway, clamping will decrease magma overpressure (ΔP_o is negative). Conversely, the term "unclamping" refers to a decreasing compressive normal stress on a pathway (positive $\Delta\sigma_n$), which increases P_o (positive ΔP_o). In our model, the vertical arc-parallel and arc-perpendicular pathways represent potential pathways for dykes, generally favoring upward magma transport (Rubin, 1995). Conversely, horizontal pathways represent potential pathways for sills and favor magma storage (Canales et al., 2009; Gudmundsson, 2011, 2012; Jaxybulatov et al., 2014; Menand, 2008). We use $\Delta\sigma_n$ on these pathways as a proxy for the magmatic response and present six mechanisms showing how clamping and unclamping may impact the end-member pathways (Figure 2).

Clamping of pathways decreases P_o, effectively acting as a stress barrier to magma transport. This inhibits intrusion propagation and decreases intrusion thickness and therefore magma flow rate (Gudmundsson, 1986; A. Gudmundsson, 2020). However, clamping of existing vertical intrusions may initially cause some magma ascent if the intrusion is connected to shallower parts of the system. This is because narrowing of the intrusion will be opposed by an increase in the internal magma pressure, which may subsequently dissipate by magma flow up and out of the intrusion (Figure 2, mechanism 1: Feuillet et al., 2011; Rikitake & Sato, 1989). However, clamping of vertical pathways is generally expected to discourage magma ascent in dykes (Figure 2, mechanism 2), while clamping of horizontal pathways (increasing compressive vertical stress) is expected to discourage magma storage by inhibiting sill formation.

Conversely, unclamping of pathways increases P_o, favoring intrusion propagation and causing intrusion opening thickness to increase. Unclamping of vertical pathways therefore favors magma ascent in dykes, perhaps especially so when the magnitude of unclamping increases toward shallower depths, as this generates a favorable pressure gradient for magma ascent (Figure 2, mechanism 3: Bonali et al., 2013; Dahm, 2000; Hill et al., 2002; Nostro et al., 1998). Unclamping of horizontal pathways (decreasing compressive vertical stress) favors magma storage in sills. Unclamping of horizontal pathways also encourages dyke deflection into sills, as the decreased vertical stress makes it easier for the tensile stress ahead of a propagating dyke tip to open up mechanically weak horizontal structures such as layering (Figure 2, mechanism 4: A. Gudmundsson, 2011). However, unclamping of sills increases P_o which may lead to failure of the sill walls. Depending on the local stress field, dyke injection upon failure is possible which will lead to magma ascent, although injection of further sills and growth of the magma storage zone may occur instead (Albino et al., 2010; Grosfils, 2007).

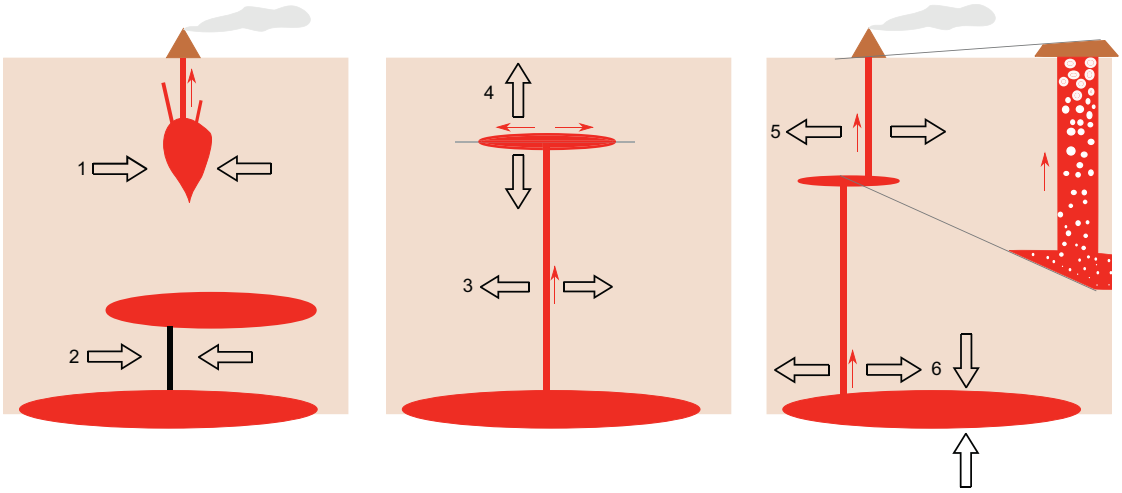

Figure 2. Simplified, not-to-scale diagram showing the following mechanisms for static normal stress changes affecting planar magma bodies. (1) Clamping expels magma upwards from existing intrusions while (2) impeding magma from entering new or existing pathways. (3) Unclamping of vertical pathways encourages magma ascent in dykes, while (4) unclamping of horizontal pathways favors magma storage in sills. (5) Unclamping or volumetric expansion at shallow depths may encourage volatile exsolution and increase magma buoyancy. (6) Intersections of clamped horizontal magma reservoirs with unclamped vertical pathways may be especially favorable for upwards magma transport.

At shallower depths, unclamping of intrusions (or volumetric expansion in σ_{kk}) may trigger volatile exsolution and thereby decrease the density of the magma, favoring magma ascent due to buoyancy (Figure 2, mechanism 5: Hill et al., 2002; Walter & Amelung, 2007). Intersections between intrusions may also be important. Clamping of sill-like (horizontal) magma reservoirs may encourage flow of magma out of those reservoirs, potentially upwards into intersecting unclamped vertical intrusions, greatly favoring magma ascent (Figure 2, mechanism 6). Considering these six mechanisms, we suggest that, in general, magma ascent is favored by clamping of horizontal pathways and unclamping of vertical pathways, while magma stalling and storage is favored by clamping of vertical pathways and unclamping of horizontal pathways. However, while these mechanisms are plausible and intuitive, observational evidence of their operation is currently unclear.

The response of the magmatic system depends on both the static stress change and the background stress field. Subduction zone interface earthquakes relax compressional stresses accumulated perpendicular to the plate boundary. Unclamping of arc-parallel pathways is therefore expected to be the main response, which will favor magma ascent, but the previously uninvestigated stress changes on arc-perpendicular and horizontal pathways may also be important. Coseismic unclamping has previously been invoked to explain magmatism occurring along arc-parallel structures that are unfavorably orientated within a compressive stress field with σ_1 perpendicular to the plate boundary (Acocella, 2014; Acocella et al., 2018; Bonali et al., 2013; Lara et al., 2006; Lupi & Miller, 2014; Mpodozis & Cornejo, 2012; Sepúlveda et al., 2005; Walter & Amelung, 2007).

3. Model Setup

3.1. Earthquake Ruptures

We use Coulomb 3 to calculate static stress changes caused by earthquake ruptures in an isotropic elastic halfspace (Lin & Stein, 2004; Toda et al., 2005). Coulomb 3 uses the equations of Okada (1992) to calculate the displacement field surrounding a finite rectangular dislocation, from which the stress change tensor field is calculated using Hooke's Law. We model subduction interface earthquakes: thrust earthquakes that occur along the seismogenic boundary between the subducting slab and the overriding continental crust. We begin with an idealized moment magnitude (M_w) 8 model earthquake to illustrate the general static stress changes associated with subduction interface events, before presenting idealized earthquakes with M_w from 6 to 9. The effect of altering the dip of the subduction interface is also investigated. Finally, we

present an example using a slip distribution model from a real subduction interface earthquake. The idealized models are independent of the chosen Young's modulus and we use a Poisson's ratio of 0.25. Models with variable Poisson's ratio, slip distribution, and rupture scaling laws are presented in the supplementary information (Figures S2–S4).

The source characteristics of subduction zone interface earthquakes vary between and within subduction zones due to heterogeneity in subduction geometry, mechanical properties of the interface, and stress distribution, among others (Schellart & Rawlinson, 2013). The idealized models consider the simple case of a pure thrust earthquake with zero along-strike displacement and a uniform slip distribution. Pure thrust earthquakes may occur during orthogonal subduction, where the plate convergence vector is perpendicular to the plate boundary. Oblique convergence may also produce pure thrust earthquakes when strain is partitioned into thrusting and strike-slip faulting domains.

To generate the idealized models, we use global datasets of subduction zones (Hayes et al., 2018; Heuret et al., 2011; Pacheco et al., 1993; Tichelaar & Ruff, 1993) to define a typical subduction zone interface on which the model thrust earthquakes occur. We find a mean interface dip of 20 degrees and choose an upper boundary of the seismogenic zone of 5 km (Table S1). Above 5 km, stable sliding is assumed to occur due to the presence of nonseismogenic sediment layers (Vrolijk, 1990; Moore & Saffer, 2001). We chose a shallower depth to the top of the seismogenic zone than suggested by the global datasets as large earthquakes often rupture far into the upper stable zone (Kanamori & Kikuchi, 1993).

Many scaling relationships exist for subduction zone earthquake rupture dimensions (e.g., Allen & Hayes, 2017; Blaser et al., 2010; Murotani et al., 2013; Skarlatoudis et al., 2016; Strasser et al., 2010; Thingbaijam et al., 2017). The along-strike rupture length (L) versus M_w relationship is relatively well-defined and consistent, but there is more variability in the down-dip rupture width (W) versus M_w relationships (Allen & Hayes, 2017). We use the scaling relationships derived by Strasser et al. (2010), which are empirically derived, linear, nonself-similar, and lie roughly in the middle of existing scaling relationships (Allen & Hayes, 2017). Although there is sound empirical and theoretical evidence for width-saturation of the seismogenic zone for larger subduction earthquakes (Allen & Hayes, 2017; Hyndman et al., 1997; Tajima et al., 2013), disregarding this helps preserve the simplicity of our model.

For each idealized model earthquake magnitude, L and W are obtained from the relationships of Strasser et al. (2010), before the amount of reverse slip (S) on the interface is calculated by

$$S = \frac{10^{\frac{3}{2}(M_w+6.06)}}{\mu WL}, \tag{9}$$

where μ is the shear modulus (all parameters in SI units). As the rupture dimensions are fixed and the model space is isotropic, the resulting static stress changes are independent of the Young's modulus; any increase to the Young's modulus is canceled out by a corresponding decrease to the applied slip. Although the scaling relationships of Strasser et al. (2010) do not enforce self-similar scaling, we initially use the stress field changes produced by the M_w 8 idealized model earthquake as an example, under the assumption that the spatial patterns of stress field changes produced by the other idealized models will be generally similar, only acting over correspondingly different spatial scales and magnitudes (Wells & Coppersmith, 1994).

3.2. Model Geometry

The geometries of the model and end-member pathways are as previously described (Figure 1). The oceanic trench marks where the up-dip projection of the rupture plane intersects the surface $z = 0$; the midpoint of the trench defines the point [0 0 0] within the model wireframe. The x-axis is positive away from the oceanic trench in the direction of dip. Parameter values for each idealized model earthquake magnitude are shown in Table S2.

Although magmatic intrusions may occur in any orientation, we use the arc-parallel and arc-perpendicular end-members as these are easily defined relative to the subduction zone tectonics. Further, intrusions may exploit pre-existing structures that act as planes of weakness in the orientations defined by our end-mem-

ber pathways (Cembrano & Lara, 2009; Richards et al., 2001; Tosdal & Richards, 2001). Arc-parallel pathways may represent dykes formed in volcanic arcs undergoing extension due to slab rollback, or intrusions which exploit strike-slip faults or shear zones commonly found within volcanic arcs that accommodate any oblique convergence (e.g., Cembrano et al., 1996). Arc-perpendicular pathways may represent the path of least resistance for dykes formed under compressional subduction tectonics, or intrusions which exploit tear faults or so-called cross-arc lineaments of unclear nature (Salfity, 1985; Salfity & Gorustovich, 1998). Horizontal pathways may represent sills or magma bodies formed under strongly compressional settings, or due to the presence of rheological or density layering within the crust which create suitable conditions for sill formation in other tectonic environments (A. Gudmundsson, 2011; Rivalta et al., 2015).

The normal stress changes on the end-member pathways are calculated at every point within the 3D model wireframe, however, it is important to consider the location of potential magmatic activity. Dickinson (1973) states that the distance between oceanic trenches and associated volcanic arcs ranges from 100 to 300 km. However, several present-day volcanic arcs lie toward the upper end of, or beyond, this range (e.g., Chile and Sumatra: Walter & Amelung, 2007; Acocella et al., 2018). An analysis using the Smithsonian Global Volcanism database (Global Volcanism Program, 2013) found a global mean trench-to-arc distance of 287 ± 161 km (Pall et al., 2018). This analysis suggests ≈ 84% of global subduction zone volcanoes should be located within 448 km of the oceanic trench. We therefore refer to the area between 100 and 500 km from the oceanic trench in the x-direction as the zone of likely magmatism (ZLM) and focus our interpretation and discussion on this area (Figure 1).

4. Modeled Normal Stress Changes

The normal stress changes on the three end-member pathways and the mean stress change are shown for the M_w 8 model earthquake in map view at 5 km depth (Figures 3e–3h) and in cross-section through the center of the rupture (Figures 4e–4h). The normal stress change depends on both the strain normal to the pathway and the volumetric strain. As ϵ_{xx} is the dominant strain component (Figures 3a and 4a), the volumetric strain (ϵ_{kk}: Figures 3d and 4d) strongly resembles ϵ_{xx}. The normal stress change on arc-parallel pathways ($\Delta\sigma_{xx}$: Figures 3e and 4e), therefore strongly resembles the induced strain ϵ_{xx}. Arc-parallel pathways are generally unclamped within the ZLM, although clamping occurs beyond the lateral rupture tips (Figure 3e). Beyond the down-dip rupture tip, the magnitude of unclamping increases toward the surface, whereas closer to and above the rupture itself, the magnitude of unclamping generally increases with depth toward the rupture (Figure 4e).

As there is no slip on the rupture plane in the y-direction, ϵ_{yy} is largely induced to counteract stress changes resulting from displacements in the x-direction, as well as directly counteracting ϵ_{xx} due to the non-zero Poisson's ratio; where there is extension in ϵ_{xx} adjacent to the rupture plane (Figure 3a), there is a corresponding contraction in ϵ_{yy} (Figure 3b) and where there is contraction in ϵ_{xx} beyond the lateral rupture tips there is a corresponding extension in ϵ_{yy}. As ϵ_{yy} is the smallest component of induced strain, the stress changes on arc-perpendicular pathways ($\Delta\sigma_{yy}$: Figures 3f and 4f) are most strongly influenced by ϵ_{kk}. Contraction in ϵ_{yy} in the ZLM (Figure 4b) is counteracted by volumetric expansion (Figure 4d), resulting in very small stress changes in σ_{yy} over much of the ZLM (Figure 4f). However, arc-perpendicular pathways are unclamped above the down-dip rupture tip, with the magnitude of unclamping increasing with depth. Beyond the along-strike rupture tips, extension in ϵ_{yy} (Figure 3b) causes unclamping of arc-perpendicular pathways, with the magnitude of unclamping increasing toward the surface (Figure 3f).

The induced normal strain ϵ_{zz} depends on the relative magnitudes of slip in the z-direction on the rupture plane and the movement of the free-surface in the z-direction. Above the rupture plane, vertical (upwards) displacement on the rupture surface dominates over the uplift of the free surface, thus causing contraction in ϵ_{zz} (Figure 4c); this causes clamping of horizontal pathways above the rupture plane ($\Delta\sigma_{zz}$: Figure 4g). Beyond the down-dip rupture tip, subsidence is largest at the free surface and decays with depth, therefore also causing contraction in ϵ_{zz} (Figure 4c). However, contraction beyond the down-dip rupture tip (Figure 3c) is largely counteracted by volumetric expansion (Figure 3d), resulting in only a small lobe of clamping of horizontal pathways beyond the down-dip rupture tip, which transitions to unclamping at greater distances away from the rupture (Figure 4g). Above the down-dip rupture tip, there is a lobe of extension in ϵ_{zz} which

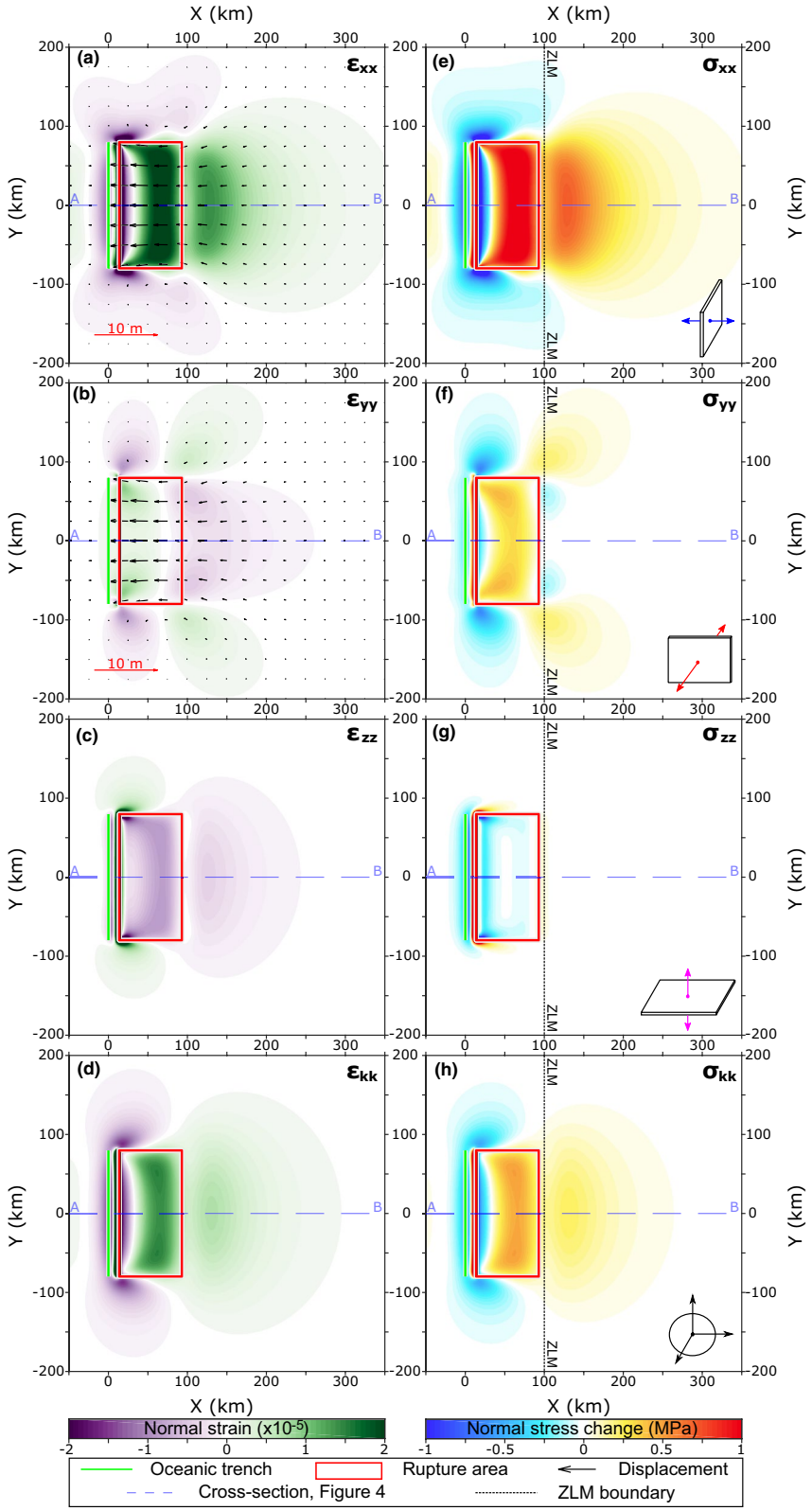

Figure 3. (a–c) The three components of normal strain, and (d) the volumetric strain induced by the M_w 8 model earthquake, shown in map view at 5 km depth (depth to top of rupture). The arrows show the displacement field projected onto the xy plane at 5 km depth in (a and b) to show how the strains ϵ_{xx} and ϵ_{yy} arise. (e–g) The three components of normal stress change on end-member pathways, and (h) the mean stress change for the M_w 8 model earthquake model. The zone of likely magmatism is located in the area x = 100–500 km.

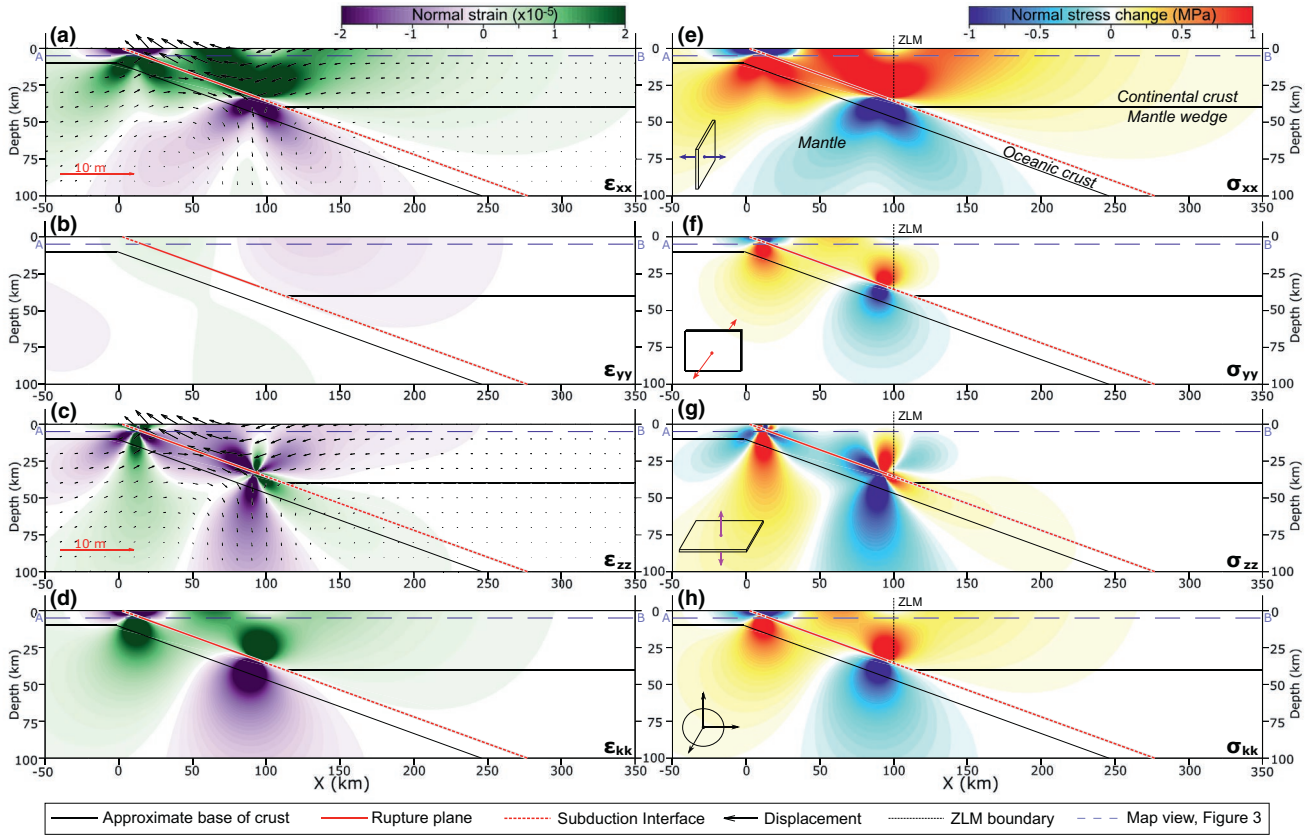

Figure 4. (a–c) The three components of normal strain, and (d) the volumetric strain induced by the M_w 8 model earthquake, shown in cross-section through the center of the rupture along the line $y = 0$. The arrows show the displacement field projected onto the xz plane at $y = 0$ in (a and c) to show how the strains ϵ_{xx} and ϵ_{zz} arise. (e–g) The three components of normal stress change on end-member pathways, and (h) the mean stress change for the M_w 8 model earthquake model. The zone of likely magmatism is located above the subduction interface at $x = 100$–500 km.

combines with volumetric expansion in the same area (Figure 4d) to produce a strong lobe of unclamping of horizontal pathways (Figure 4g). By definition, the normal stress change on horizontal pathways at $z = 0$ is zero.

5. Stress Change Regimes

5.1. Motivation and Method

At each model grid point, we generate profiles of normal stress change on the end-member pathways versus depth. By analyzing those profiles that lie within the ZLM, we identify stress change regimes that display specific combinations of stress change on the end-member pathways with depth (e.g., Figures 5b–5i). Defining these regimes simplifies the otherwise complex stress change field, allowing the patterns in stress change to be mapped out spatially (Figure 5a) and facilitating interpretation of whether each regime will favor magma storage or ascent. The regimes were originally defined using the M_w 8 idealized model and then refined using the different idealized models as well as real earthquake models. In total, we identify seven stress change regimes and two sub-regimes (Table 1).

Stress change regime assignment is automatically computed using the regime requirements as listed in Table 1. The stress change profiles are analyzed to the depth of the subduction interface or 100 km, whichever is shallowest. Regime assignment requires ≥10 depth intervals above the subduction interface; for the z-increment of 2 km used here, this corresponds to a minimum depth to the subduction interface of 18 km for stress regime calculation. Additionally, the maximum normal stress change in each profile must exceed

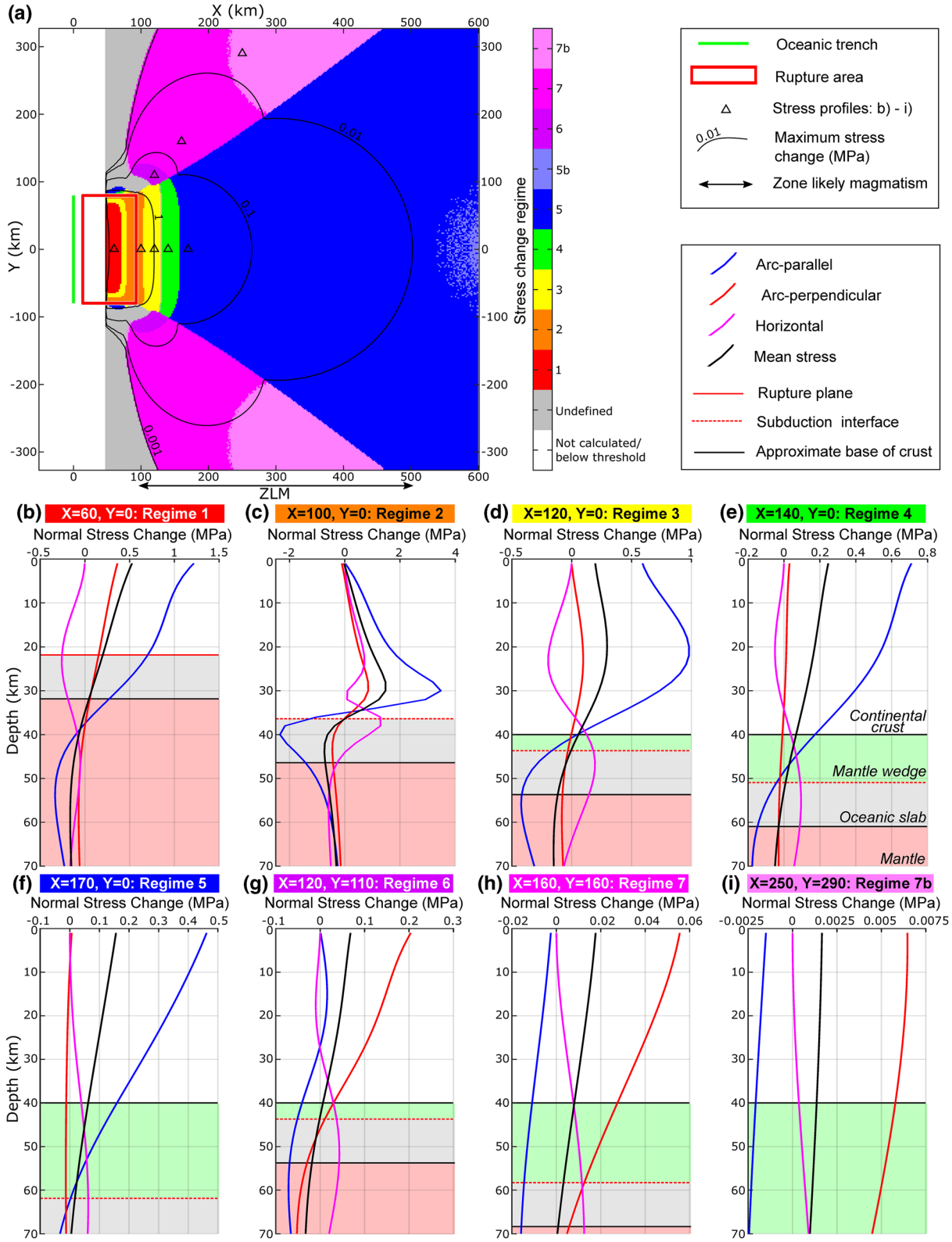

Figure 5. Stress change regimes based on the stress changes with depth on end-member pathways for the M_w 8 idealized model earthquake. (a) Spatial distribution of the stress change regimes. Regimes are not calculated at $x < 50$ km, due to shallowing of the subduction interface toward lower x values. Contours show the maximum normal stress change on any end-member pathways above the subduction interface. (b–i) Stress changes on end-member pathways versus depth profiles for the M_w 8 idealized model earthquake. The locations of the profiles are shown by the triangles in (a). Note the different horizontal scale for each profile.

Table 1
Summary of Stress Change Regimes

Regime	Arc-parallel	Arc-perpendicular	Horizontal	Location and notes
1	**Unclamping:** Maximum value at surface	(Unclamping: Increasing toward surface)	Clamping: Peak at subduction interface	Above the rupture plane
2	**Unclamping:** Increasing with depth*	(Unclamping: Increasing with depth*)	(Unclamping: Increasing with depth*)	Above the down-dip rupture tip. ∗Peak unclamping occurs at ≥75% depth to subduction interface. May transition to clamping very near the subduction interface
3	**Unclamping:** Peak in mid continental crust	(Unclamping: Peak in mid continental crust)	Clamping: Peak in mid continental crust	Either side of the down-dip rupture tip.
4	**Unclamping:** Increasing toward surface	(Unclamping/clamping: Increasing toward surface)	Clamping: Peak in mid-continental crust*	Beyond down-dip rupture tip. ∗May transition to unclamping at greater depths
5	**Unclamping:** Increasing toward surface*	(Unclamping/clamping: Increasing toward surface)	Unclamping: Increasing with depth	Further beyond the down-dip rupture tip. ∗Regime 5b where the value at the surface is not the largest, but still ≥90% maximum value
6	(Variable)	**Unclamping:** Increasing toward surface	Clamping: Peak in mid-continental crust	Beyond the lateral rupture tips.
7	(Variable)	**Unclamping:** Increasing toward surface*	Unclamping: Increasing with depth	Beyond the lateral rupture tips. ∗Regime 7b where the value at the surface is not the largest, but still ≥90% maximum value.

Note. Parentheses indicate a typical stress change for that regime, but not a requirement. Bold text indicates the largest magnitude stress change in each regime. The stress change on arc-perpendicular pathways in Regimes 3–5 is typically very low magnitude, with clamping or unclamping determined by the rupture aspect ratio.

a minimum stress change threshold value of 10^{-3} MPa, which is on the order of solid Earth tidal stress changes (Cochran et al., 2004), with any smaller stress changes assumed to be insignificant.

5.2. Regime Definitions

Regimes 1–5 occupy the area roughly adjacent to the earthquake rupture and are characterized by unclamping of arc-parallel pathways as the largest magnitude stress change. The gradient with depth of this unclamping, as well as the stress changes on horizontal pathways, differs between these regimes. The stress changes on arc-perpendicular pathways in Regimes 1–5 depend strongly on the rupture aspect ratio but are generally very low magnitude and are not used in the assignment of these regimes (Figure S1). The spatial distribution of Regimes 1–5 relates to the location of the down-dip rupture tip, where stress change is concentrated. Near the down-dip rupture tip, stress changes increase downwards toward the subduction interface (Regime 2). Moving away from the rupture tip, the peak stress changes on arc-parallel pathways occur at progressively shallower levels, moving from the mid-continental crust (Regime 3), to the surface (Regimes 1, 4, and 5). Regimes 6 and 7 are located beyond the lateral faults tips and are characterized by unclamping of arc-perpendicular pathways as the largest stress change. Regimes 6 and 7 are differentiated by the stress change on horizontal pathways. Regimes 5 and 7 cover the greatest spatial extent, while Regimes 1–4 and 6 occupy a much smaller area closer to the rupture itself. The undefined region in Figure 5a is an area of highly variable stress changes, due to proximity to both the down-dip and lateral rupture tips.

Regime 1 occurs in the region around the center of the rupture. The maximum unclamping on arc-parallel pathways occurs at the shallowest depth, reaching values of >1 MPa at 1 km depth in the M_w 8 example (Figure 5b). The magnitude of unclamping generally increases upwards from the subduction interface toward the surface. Horizontal pathways are clamped in Regime 1, with peak clamping occurring at the subduction interface at values of <0.5 MPa for the M_w 8 model. Arc-perpendicular pathways are generally increasingly unclamped toward the surface, although with lower magnitudes (<0.5 MPa for the M_w 8 model) than the arc-parallel pathways.

Regime 2 has the largest stress change magnitudes of any regime, with up to several MPa of unclamping on arc-parallel pathways for the M_w 8 model. These high stress change values occur as Regime 2 is located near the down-dip rupture tip. The peak unclamping of arc-parallel pathways occurs near the base of the continental crust (≥75% of the depth to the subduction interface), with a magnitude more than twice that at the shallowest depth (Figure 5c). All three end-member pathways are generally increasingly unclamped with depth toward the subduction interface, although below the depth of peak unclamping there may be a sharp reduction in the stress change and perhaps even a transition to clamping, especially for the horizontal pathways. Arc-perpendicular pathways show the same unclamping pattern as the arc-parallel pathways, suggesting that $\Delta\sigma_{yy}$ is mainly controlled by the volumetric expansion dominated by ϵ_{xx}.

Regime 3 occurs either side of Regime 2 at the down-dip rupture tip. The maximum unclamping of arc-parallel pathways is at intermediate depths, at less than 75% of the depth to the subduction interface but below the surface (Figure 5d). Horizontal pathways are clamped, with peak clamping also occurring at an intermediate depth between the surface and the subduction interface. The stress changes on arc-perpendicular pathways again match those on arc-parallel pathways, but with lower magnitudes. In the M_w 8 model, peak unclamping on arc-parallel pathways reaches around 1 MPa, while the stress changes on horizontal and arc-perpendicular pathways are lower.

Regimes 4 and 5 are located beyond the down-dip rupture tip and are characterized by increasing magnitudes of unclamping on arc-parallel pathways toward the surface. Peak unclamping values at 1 km depth are around 0.7 MPa in Regime 4 (Figure 5e) and 0.5 MPa in Regime 5 (Figure 5f) for the M_w 8 model. Horizontal pathways are clamped in Regime 4, with peak clamping at intermediate depths. The magnitude of clamping of horizontal pathways is lower in Regime 4 than in Regime 3, and there may be a transition to unclamping at greater depths closer to the subduction interface. In Regime 5, horizontal pathways are unclamped, with the magnitude of unclamping increasing with depth toward the subduction interface. The stress changes on arc-perpendicular pathways are more than an order of magnitude smaller than those on arc-parallel pathways in Regimes 4 and 5. At especially great distances from the rupture, there is a reduction in the magnitude of unclamping on arc-parallel pathways at shallow depths in Regime 5. Hence, we define Regime 5b, which is the same as Regime 5 but with an allowance for up to 10% reduction in unclamping at the surface, relative to the maximum unclamping value.

In Regimes 6 and 7, the maximum stress change occurs on arc-perpendicular pathways. Regimes 6 and 7 are located beyond the lateral rupture tips, with Regime 6 adjacent to the near-fault Regimes 1–4, whereas Regime 7 occupies large areas adjacent to Regime 5. Unclamping of arc-perpendicular pathways increases toward the surface in both Regimes 6 and 7, reaching up to 0.2 MPa in the M_w 8 example in Regime 6 (Figure 5g), but an order of magnitude lower in Regime 7 (Figure 5h). In Regime 6, horizontal pathways are clamped with peak clamping at intermediate depths. In Regime 7, horizontal pathways are unclamped, with the magnitude of unclamping increasing with depth toward the subduction interface. Across Regimes 6 and 7, the stress changes on arc-parallel pathways are more variable, showing both clamping and unclamping depending on depth and the distance from the rupture. At large distances from the rupture, Regime 7b is defined where, as with Regime 5b, there is up to a 10% reduction in unclamping of arc-perpendicular pathways at the surface relative to the peak unclamping value.

5.3. Controls on Regime Distribution

5.3.1. Earthquake Moment Magnitude

Large earthquakes are assumed to be fundamentally similar to small earthquakes (e.g., Kanamori & Anderson, 1975), so similar stress field changes are expected for different magnitude idealized subduction interface earthquakes, only acting over spatial scales corresponding to their rupture dimensions. The stress regime maps in Figure 6 show similar spatial distributions of stress change regimes for idealized earthquake models of M_w of 6–9. With increasing M_w, more of the ZLM is covered by the defined stress change regimes; larger earthquakes exhibit greater slip magnitudes and therefore generate larger stress changes at comparable distances. Furthermore, stress change amplitude decays as a power law with distance away from the rupture plane and so large earthquakes generate strong stress changes over a larger crustal volume. The increased down-dip rupture width of larger earthquakes also causes the down-dip rupture tip to move

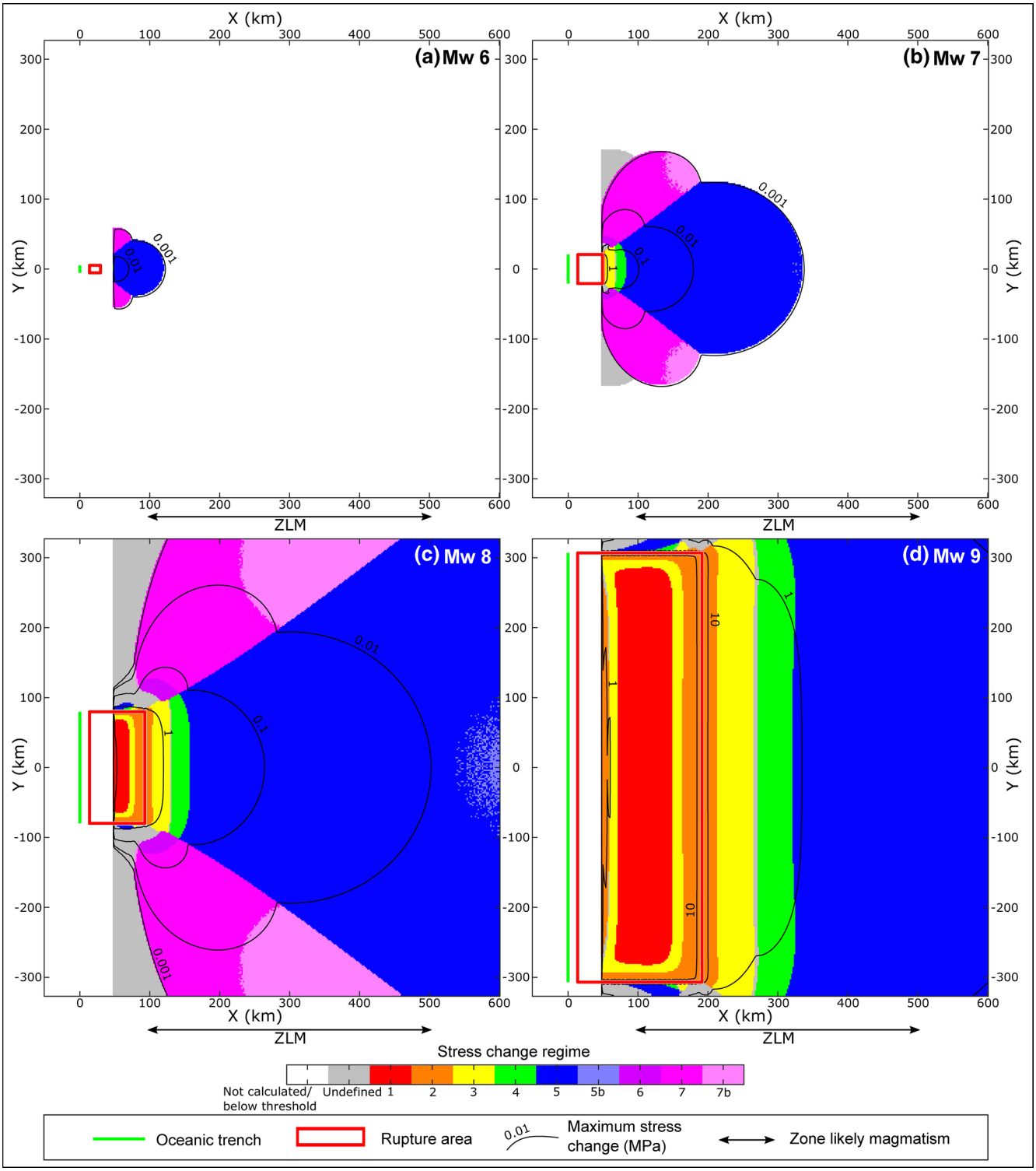

Figure 6. Spatial distributions of stress change regimes for different magnitude idealized earthquake models: (a) M_w 6, (b) M_w 7, (c) M_w 8, and (d) M_w 9. Regimes are not calculated at $x < 50$ km, due to shallowing of the subduction interface toward lower x values. Contours show the maximum normal stress change on any end-member pathway above the subduction interface.

to greater depths. With a deeper source of stress concentration, the width of the stress change regimes at the surface therefore increases with increasing earthquake magnitude. The contours in Figure 6 show the maximum value of unclamping on any end-member pathway above the subduction interface. While the orientation and gradient with depth of stress changes within a particular regime are the same regardless of earthquake magnitude, the magnitude of the stress changes varies with earthquake magnitude and distance to the rupture (Figures S5–S7). For example, in the M_w 7 model, only Regimes 5, 7, and 7b are located within the ZLM with stress change magnitudes of < 0.1 MPa. In the M_w 9 model, every stress change regime is located within the ZLM, with magnitudes commonly >1 MPa.

5.3.2. Subduction Interface Dip

We use a minimum interface dip of 9 degrees and a maximum dip of 35 degrees (Table S1) to investigate the effects of changing interface dip on the stress change regimes. Varying the interface dip considerably alters the near-fault distribution of the stress change regimes (Figure 7). Increasing the interface dip shifts the down-dip rupture to greater depths, thus causing wider regimes at the surface. This also means the magnitude of unclamping of arc-parallel pathways is larger for more steeply dipping subduction interfaces than more shallowly dipping ones at large trench-arc distances, even though there is less slip in the x-direction for more steeply dipping interfaces. The normal stress change on horizontal pathways is less affected.

5.3.3. Slip Distribution—Real Earthquakes

Finite fault models inverted from real earthquakes typically include variability in the slip distribution by dividing the rupture plane into patches with variable rake and slip magnitude. The resulting stress changes are therefore more complex than those produced by the uniform slip models, although they likely still underestimate the real-world complexity. Figure 8 shows an example of the stress regimes produced from a finite fault model of the 2010 M_w 8.8 Maule, Chile earthquake. Overall, the stress regime distribution is similar to the idealized earthquakes, although there is significant complexity introduced in the near-fault area (Figure S8).

6. Discussion

6.1. Regime Implications for Magmatic Systems

We have defined a set of stress change regimes produced by typical subduction interface earthquakes, based on the magnitude, orientation, and gradient with depth of static stress changes within the ZLM. All three of these components of the static stress change may have implications for any potential impact on magmatic systems. We focus our discussion on how the different stress change regimes may favor either magma storage or ascent. Regimes which favor magma ascent are more likely to lead to volcanic unrest and possibly eruption. In general, clamping of vertical pathways and unclamping of horizontal pathways is expected to favor magma storage, whereas clamping of horizontal pathways and unclamping of vertical pathways will favor magma ascent. Unclamping of vertical pathways which increases in magnitude toward the surface may also generate a favorable pressure gradient for magma ascent.

Larger earthquakes produce strong static stress changes over the greatest crustal volume and so have greater potential to affect magmatic systems. However, we also highlight the importance of the spatial distribution of the stress changes regimes. For a given earthquake magnitude, the greatest stress changes occur in Regime 2 near the base of the continental crust. The peak stress changes in the relatively narrow Regime 2 are around an order of magnitude greater than in any other regime. In Regime 2, peak unclamping of all pathways generally occurs near the base of the continental crust, producing a large positive mean stress change with high potential to disturb magmatic bodies accumulated near the base of the crust (e.g., Annen et al., 2006; Hildreth & Moorbath, 1988). However, due the narrowing of the lobe of unclamping of horizontal pathways above the down-dip rupture tip (Figure 4g), some areas in Regime 2 display a reduction in unclamping or a transition to clamping of horizontal structures near the subduction interface (e.g., Figure 5c). While this causes a reduction in the overall expansion, the combination of very high magnitude unclamping of vertical pathways and clamping or low magnitude unclamping of horizontal pathways may create favorable conditions for ascent of magmas from the lower crust.

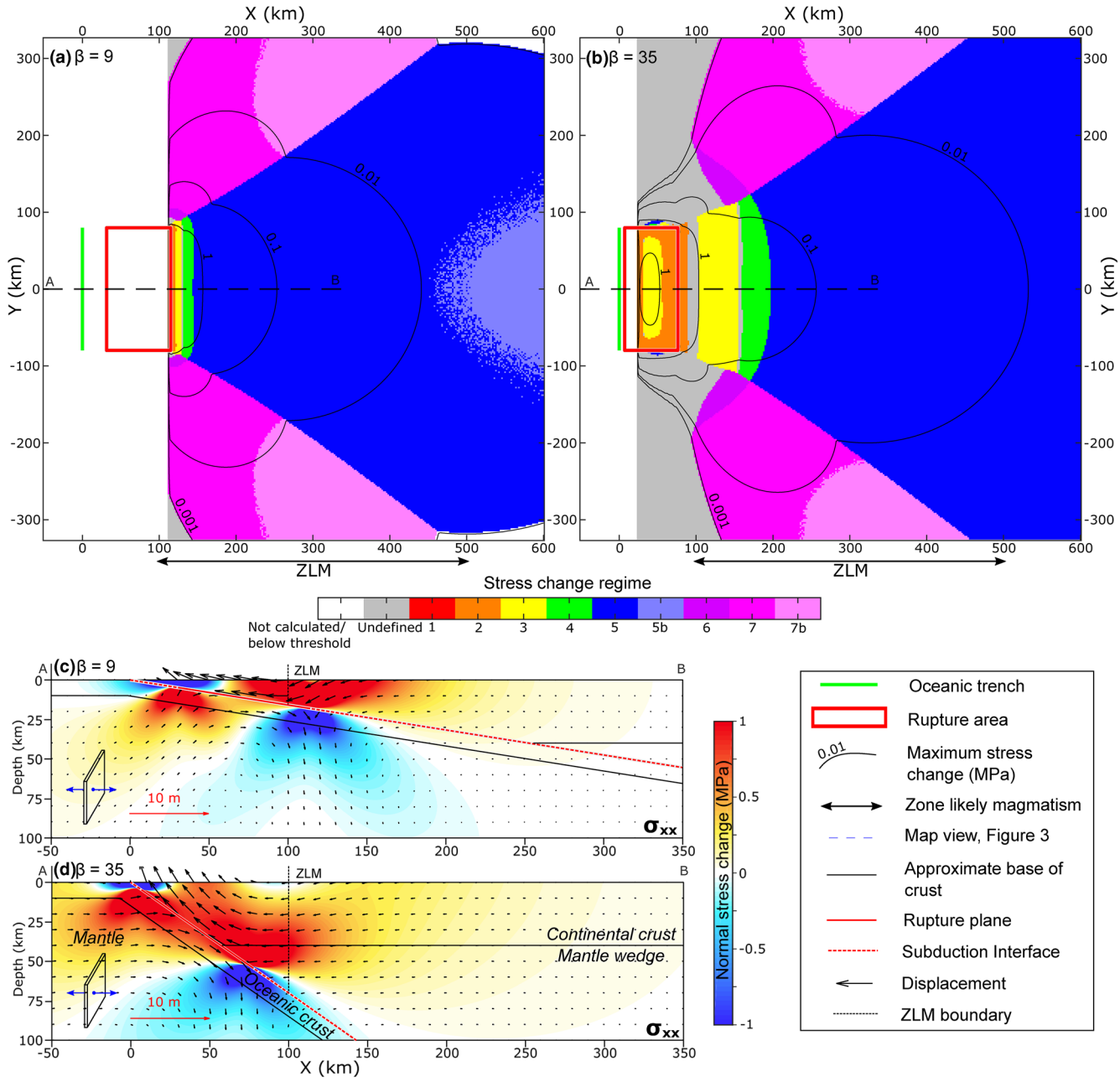

Figure 7. Spatial distribution of stress change regimes for the M_w 8 model earthquake on an interface with dip of (a) 9 degrees and, (b) 35 degrees. Contours show the maximum normal stress change on any end-member pathway above the subduction interface. Cross sections along the line A-B, showing the normal stress change on arc-parallel structures and the displacements projected onto the *xz* plane are shown in (c) for the 9° interface and (d) for the 35° interface.

Regimes 1, 4, and 6 also display characteristics which may strongly favor magma ascent. Regime 4 combines clamping of horizontal pathways with unclamping of arc-parallel pathways that increases in magnitude toward the surface. This combination of stress changes may be especially favorable for encouraging flow of magma out of horizontal reservoirs and upwards into vertical dykes. Regime 1 stress changes are very similar to Regime 4, however, Regime 1 stress changes may not be very widespread in real-world scenarios (Figure 8). Regime 6 combines clamping of horizontal pathways with unclamping of arc-perpendicular pathways that increases in magnitude toward the surface. Although the magnitudes of stress change are lower in Regime 6 than in Regime 4, unclamping of arc-perpendicular pathways may be important in com-

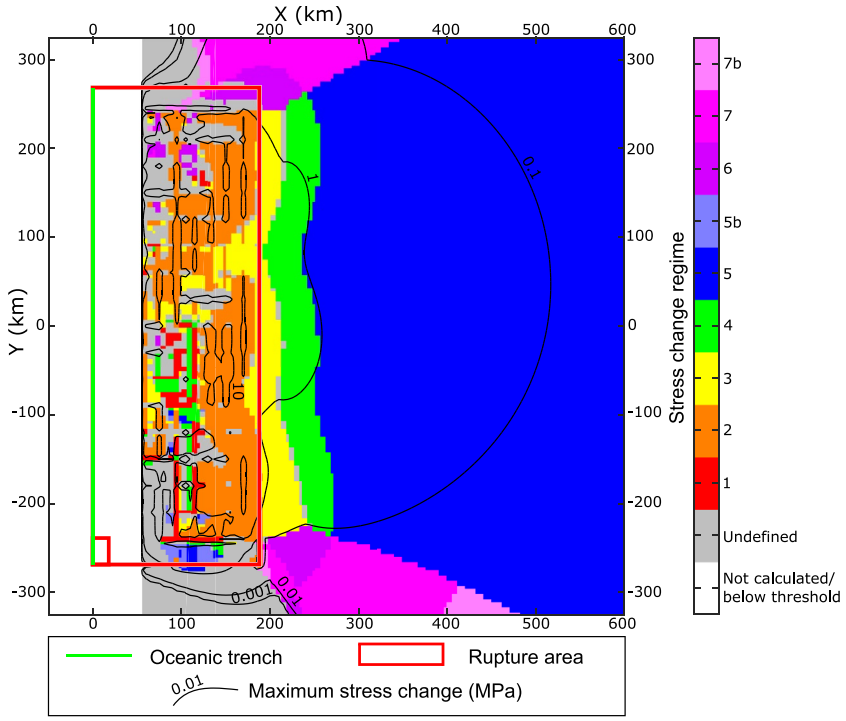

Figure 8. Stress change regimes for the 2010 M_w 8.8 Maule Chile earthquake, using the finite fault model of Hayes (2010) from the NEIC (http://earthquake.usgs.gov/earthquakes/eventpage/official20100227063411530_30/finite-fault). The size of each individual slip patch is shown by the slip patch in the bottom left corner of the rupture plane, the other slip patches have been removed for clarity. Note the near fault complexity in the stress change regimes, especially in Regimes 1 and 2, with Regime 1 especially poorly produced. This complexity is also shown by the 10 MPa stress change contour within the rupture area. Young's modulus of model is 80 GPa.

pressive volcanic arcs where pre-existing cross-arc structures are more favorably orientated for fluid flow than arc-parallel structures (e.g., Cembrano & Lara, 2009; Lara et al., 2006).

Regime 3 combines moderate magnitude clamping of horizontal pathways and unclamping of arc-parallel pathways in the mid-crust, which may encourage magma ascent. Regime 5 exhibits unclamping of arc-parallel pathways which increases in magnitude toward the surface, while Regime 7 displays unclamping of arc-perpendicular pathways which increases toward the surface, both of which may encourage magma ascent. However, horizontal pathways are unclamped at depth in Regimes 5 and 7, which may encourage accumulation of magma near the base of the crust, favoring magma storage at depth. Although the magnitudes of stress change are lowest in Regimes 5 and 7, they cover the largest area. Thus, while subduction thrust earthquakes generally encourage magma ascent by unclamping vertical pathways, large areas of the volcanic arc may experience unclamping of horizontal pathways at depth.

6.2. Threshold Stress Changes

In studies of earthquake triggering, a Coulomb static stress change value of 0.1 MPa is sometimes used as a threshold value, above which the triggering of earthquakes might be expected (Freed, 2005; Grasso & Sornette, 1998; Mulargia & Bizzarri, 2014). Adopting this as a threshold for affecting magmatic systems, $M_w > 7$ earthquakes are required to produce static stress changes exceeding the threshold within the ZLM, with $M_w > 8$ earthquakes required to produced 0.1 MPa stress changes at more typical trench-arc distances of 200–300 km (Figure 6). Other studies suggest a lower threshold value of 0.01 MPa (Hardebeck et al., 1998; King et al., 1994; Reasenberg & Simpson, 1992), while some suggest that a threshold value does not exist and that seismicity rate obeys the rate-state friction law for coulomb stress changes of 1 kPa or less (Kilb et al., 2002; Scholz et al., 2019; Ziv & Rubin, 2000). Therefore, any magnitude of stress change could in theory induce a change in some part of the magmatic system. However, stress changes lower than the twice-dai-

ly tidal peak values on the order of 10^{-3} MPa may be considered insignificant, meaning subduction interface earthquakes of $M_w < 7$ are unlikely to affect magmatic systems. This may explain the lack of correlation between smaller earthquakes and volcanic eruptions (e.g., Sawi & Manga, 2018).

Larger stress changes will push a greater proportion of the system above any given failure threshold (or alternatively, suppress the system below failure) and therefore larger earthquakes have a greater likelihood of producing a significant effect (e.g., Meier et al., 2014). Without knowing the state of the magmatic system prior to the earthquake, it is impossible to say what magnitude of stress change is necessary to cause a significant effect. However, even large earthquakes may not produce detectable changes. For example, the stress change regime may favor magma storage over magma ascent, and even if the regime favors magma ascent, very few dykes ever reach the surface (A. Gudmundsson, 1984a). Hence, although there is some statistical evidence for eruption triggering (Linde & Sacks, 1998; Sawi & Manga, 2018), there may be many more currently undetectable changes in the deeper magmatic system. The state of the magmatic system at the time of the earthquake is also important, with more critically stressed systems that are closer to eruption more likely to be significantly affected (Watt et al., 2009).

6.3. Properties of the Magmatic System

Although we do not quantitatively model the response of the magmatic system, we consider an illustrative example of how the evolution of the volcanic arc may influence the response to static stress changes. A magma-filled crack of fixed length (e.g., a dyke connecting two magma reservoirs) will respond to changes in the external stress field by changing its opening thickness

$$w = \frac{2l\left(1-\nu^2\right)P_o}{E}, \tag{10}$$

where w is the half-thickness at the center of the crack and l is the half-length of the crack (Sneddon & Lowengrub, 1969). Making the assumption that the change in P_o is equal to the change in σ_n acting at the dyke wall (as may occur in a dyke where the internal magma pressure is buffered by a deeper magma reservoir) then the change in thickness of the dyke (Δw) caused by the earthquake is given by (increasing thickness positive)

$$\Delta w = \frac{2l\left(1-\nu^2\right)\Delta\sigma_n}{E}. \tag{11}$$

Using typical dyke aspect ratios of 100:1 to 1000:1 (A. Gudmundsson, 1984b; Kusumoto et al., 2013), and normal stress changes of 0.1–1 MPa (typical for M_w 8 and M_w 9 earthquakes respectively), Δw will increase on the order of 0.02%–2%, using ν of 0.25 and E of 80 GPa (e.g., Bonali et al., 2015). Although the volumetric flow rate of magma in dykes is proportional to w^3 (A. Gudmundsson, 2020), these are small changes. However, as a volcanic arc or part of a volcanic arc matures, it may heat up due to continued influx of magma and alter the mechanical properties of the system. Using a Young's modulus of 8 GPa, which may be more appropriate to heated rocks in mature magmatic systems (e.g., Bakker et al., 2016; Heap et al., 2020; Rocchi et al., 2004), the change in w will be an order of magnitude larger, potentially 20%, which will cause a significant effect on magma ascent rates. However, it should also be noted that a hotter, weaker system will act to dampen the transmission of stress changes from the earthquake, which may offset some of this effect.

6.4. Earthquakes as a Control on Magma Ascent and Storage

Magmatic processes operate across a range of timescales, from individual intrusive events, through periods of magmatic flare up, to entire magmatic epochs (De Saint Blanquat et al., 2011). Therefore, the controls on magmatic systems likely also span multiple timescales; the long-term averaged tectonic stress may be important over the lifespan of the magmatic system, whereas shorter-term changes associated with the earthquake cycle may have more of an influence on individual intrusions or pulses of magmatism.

Observing the effects of earthquakes on deep magmatic systems is challenging, however, we have suggested some possible first-order effects using an homogeneous elastic halfspace model and considering the magmatic system as a series of planar pathways. More advanced modeling should consider density and rigidity layering of the crust (A. Gudmundsson, 2006; Kavanagh et al., 2017; Maccaferri et al., 2011; Rivalta et al., 2015) and the inclusion of magma reservoirs with different geometries and time dependent, non-elastic rheologies (Albino et al., 2010; Currenti, 2018; Liao et al., 2018; Segall, 2016). The effect of the evolving crustal stress field over one or more earthquake cycles, due to processes such as viscoelastic relaxation of the lower crust, afterslip, and interseismic stress recovery is also an interesting question (e.g., Hardebeck & Okada, 2018). The role of earthquakes in influencing magma ascent and storage depends on the relative importance of static stress changes compared with other mechanisms of changing magmatic overpressures, such as magma recharge, crystallization, and volatile exsolution (e.g., Degruyter et al., 2016; Gregg et al., 2013; Tait et al., 1989). The extent to which static stress changes alter the crustal stress field is therefore an important question (e.g., Hardebeck & Okada, 2018). While earthquake-induced stress changes may likely be smaller than those caused by internal magmatic processes, the timescales over which static stress changes are applied may be much shorter.

7. Conclusions

The stress change regimes defined here may be used to better understand how magmatic systems may respond to static stress changes caused by megathrust earthquakes at subduction zones. Overall, the stress changes caused by subduction zone earthquakes favor magma ascent, since horizontal compressive stresses are relaxed. However, the more complete analysis of the stress changes performed here reveals extra complexity in the gradient with depth of horizontal stress change and in the vertical component of stress change. Notably, large regions of the volcanic arc may experience unclamping of horizontal pathways at depth, therefore favoring magma storage near the base of the crust. The responses of magmatic systems to earthquake-induced stress changes may depend on the stress change regime and magnitude experienced, as well as the state of the magmatic system, with a greater impact expected for weaker, more thermally mature volcanic arcs.

Acknowledgments
This work was supported by the Natural Environment Research Council [NE/L002434/1]. A. P. Jenkins and A. C. Rust are supported by BHP, A. P. Jenkins and J. Biggs are supported by the NERC Centre for the Observation and Modeling of Earthquakes, Volcanoes and Tectonics (COMET, http://comet.nerc.ac.uk), a partnership between UK Universities and the British Geological Survey. Comments from Agust Gudmundsson and an anonymous reviewier greatly improved this paper. Data were not used, nor created, for this research.

References

Acocella, V. (2014). Structural control on magmatism along divergent and convergent plate boundaries: Overview, model, problems. *Earth-Science Reviews*, *136*, 226–288. https://doi.org/10.1016/j.earscirev.2014.05.006

Acocella, V., Bellier, O., Sandri, L., Sébrier, M., & Pramumijoyo, S. (2018). Weak techno-magmatic relationships along an obliquely convergent plate boundary: Sumatra, Indonesia. *Frontiers in Earth Science*, *6*, 3. https://doi.org/10.3389/feart.2018.00003

Albino, F., Pinel, V., & Sigmundsson, F. (2010). Influence of surface load variations on eruption likelihood: Application to two Icelandic subglacial volcanoes, Grímsvötn and Katla. *Geophysical Journal International*, *181*(3), 1510–1524. https://doi.org/10.1111/j.1365-246X.2010.04603.x

Allen, T., & Hayes, G. (2017). Alternative rupture-scaling relationships for subduction interface and other offshore environments. *Bulletin of the Seismological Society of America*, *107*(3), 1240–1253. https://doi.org/10.1785/0120160255

Anderson, E. (1951). *The dynamics of faulting and dyke formation with applications to Britain*. Edinburgh: Oliver and Boyd.

Annen, C., Blundy, J., & Sparks, R. (2006). The genesis of intermediate and silicic magmas in deep crustal hot zones. *Journal of Petrology*, *47*(3), 505–539. https://doi.org/10.1093/petrology/egi084

Bakker, R., Frehner, M., & Lupi, M. (2016). How temperature-dependent elasticity alters host rock/magmatic reservoir models: A case study on the effects of ice-cap unloading on shallow volcanic systems. *Earth and Planetary Science Letters*, *456*, 16–25. https://doi.org/10.1016/j.epsl.2016.09.039

Becker, T., Hashima, A., Freed, A., & Sato, H. (2018). Stress change before and after the 2011 M9 Tohoku-oki earthquake. *Earth and Planetary Science Letters*, *504*, 174–184. https://doi.org/10.1016/j.epsl.2018.09.035

Biggs, J., & Pritchard, M. (2017). Global volcano monitoring: What does it mean when volcanoes deform? *Elements*, *13*(1), 17–22. https://doi.org/10.2113/gselements.13.1.17

Blaser, L., Krüger, F., Ohrnberger, M., & Scherbaum, F. (2010). Scaling relations of earthquake source parameter estimates with special focus on subduction environment. *Bulletin of the Seismological Society of America*, *100*(6), 2914–2926. https://doi.org/10.1785/0120100111

Bonali, F., Tibaldi, A., & Corazzato, C. (2015). Sensitivity analysis of earthquake-induced static stress changes on volcanoes: The 2010 M w 8.8 Chile earthquake. *Geophysical Journal International*, *201*(3), 1868–1890. https://doi.org/10.1093/gji/ggv122

Bonali, F., Tibaldi, A., Corazzato, C., Tormey, D. R., & Lara, L. E. (2013). Quantifying the effect of large earthquakes in promoting eruptions due to stress changes on magma pathway: The Chile case. *Tectonophysics*, *583*, 54–67. https://doi.org/10.1016/j.tecto.2012.10.025

Bonini, M.. (2019). Seismic loading of fault-controlled fluid seepage systems by great subduction earthquakes. *Scientific Reports*, *9*(1), 1–12. https://doi.org/10.1038/s41598-019-47686-4

Brace, W., & Kohlstedt, D. (1980). Limits on lithospheric stress imposed by laboratory experiments. *Journal of Geophysical Research*, *85*(B11), 6248–6252. https://doi.org/10.1029/JB085iB11p06248

Byerlee, J. (1978). Friction of rocks. *Pure and Applied Geophysics*, *116*, 615–626. https://doi.org/10.1007/BF00876528
Canales, J., Nedimović, M., Kent, G., Carbotte, S., & Detrick, R. (2009). Seismic reflection images of a near-axis melt sill within the lower crust at the Juan de Fuca ridge. *Nature*, *460*, 89–93. https://doi.org/10.1038/nature08095
Cashman, K., Sparks, R., & Blundy, J. (2017). Vertically extensive and unstable magmatic systems: A unified view of igneous processes. *Science*, *355*(6331), eaag3055. https://doi.org/10.1126/science.aag3055
Cembrano, J., Herve, F., & Lavenu, A. (1996). The Liquine Ofquie fault zone: A long-lived intra-arc fault system in southern Chile. *Tectonophysics*, *259*, 55–66. https://doi.org/10.1016/0040-1951(95)00066-6
Cembrano, J., & Lara, L. (2009). The link between volcanism and tectonics in the southern volcanic zone of the Chilean Andes: A review. *Tectonophysics*, *471*(1–2), 96–113. https://doi.org/10.1016/j.tecto.2009.02.038
Chaussard, E., & Amelung, F. (2014). Regional controls on magma ascent and storage in volcanic arcs. *Geochemistry, Geophysics, Geosystems*, *15*(4), 1407–1418. https://doi.org/10.1002/2013GC005216
Clemens, J., & Mawer, C. (1992). Granitic magma transport by fracture propagation. *Tectonophysics*, *204*(3–4), 339–360. https://doi.org/10.1016/0040-1951(92)90316-X
Cochran, E., Vidale, J., & Tanaka, S. (2004). Earth tides can trigger shallow thrust fault earthquakes. *Science*, *306*(5699), 1164–1167. https://doi.org/10.1126/science.1103961
Currenti, G. (2018). Viscoelastic modeling of deformation and gravity changes induced by pressurized magmatic sources. *Journal of Volcanology and Geothermal Research*, *356*, 264–277. https://doi.org/10.1016/j.jvolgeores.2018.03.020
Dahm, T. (2000). Numerical simulations of the propagation path and the arrest of fluid-filled fractures in the earth. *Geophysical Journal International*, *141*(3), 623–638. https://doi.org/10.1046/j.1365-246x.2000.00102.x
De la Cruz-Reyna, S., Tárraga, M., Ortiz, R., & Martínez-Bringas, A. (2010). Tectonic earthquakes triggering volcanic seismicity and eruptions. case studies at tungurahua and popocatépetl volcanoes. *Journal of Volcanology and Geothermal Research*, *193*(1–2), 37–48. https://doi.org/10.1016/j.jvolgeores.2010.03.005
De Saint Blanquat, M., Horsman, E., Habert, G., Morgan, S., Vanderhaeghe, O., Law, R., & Tikoff, B. (2011). Multiscale magmatic cyclicity, duration of pluton construction, and the paradoxical relationship between tectonism and plutonism in continental arcs. *Tectonophysics*, *500*(1–4), 20–33. https://doi.org/10.1016/j.tecto.2009.12.009
Degruyter, W., Huber, C., Bachmann, O., Cooper, K., & Kent, A. (2016). Magma reservoir response to transient recharge events: The case of Santorini volcano (Greece). *Geology*, *44*(1), 23–26. https://doi.org/10.1130/G37333.1
Dickinson, W. (1973). Widths of modern Arc-Trench gaps proportional to past duration of igneous activity in associated magmatic arcs. *Journal of Geophysical Research*, *78*(17), 3376–3389. https://doi.org/10.1029/JB078i017p03376
Drymoni, K., Browning, J., & Gudmundsson, A. (2020). Dyke-arrest scenarios in extensional regimes: Insights from field observations and numerical models, Santorini, Greece. *Journal of Volcanology and Geothermal Research*, *396*, 106854. https://doi.org/10.1016/j.jvolgeores.2020.106854
Ebmeier, S., Elliott, J., Nocquet, J.-M., Biggs, J., Mothes, P., Jarrín, P., et al. (2016). Shallow earthquake inhibits unrest near Chiles-Cerro Negro volcanoes, Ecuador-Colombian border. *Earth and Planetary Science Letters*, *450*, 283–291. https://doi.org/10.1016/j.epsl.2016.06.046
Ellsworth, W. (2013). Injection-induced earthquakes. *Science*, *341*(6142), 1225942. https://doi.org/10.1126/science.1225942
Feuillet, N., Beauducel, F., & Tapponnier, P. (2011). Tectonic context of moderate to large historical earthquakes in the Lesser Antilles and mechanical coupling with volcanoes. *Journal of Geophysical Research*, *116*(B10), B10308. https://doi.org/10.1029/2011JB008443
Freed, A. (2005). Earthquake triggering by static, dynamic, and postseismic stress transfer. *Annual Review of Earth and Planetary Sciences*, *33*, 335–367. https://doi.org/10.1146/annurev.earth.33.092203.122505
Global Volcanism Program. (2013). Volcanoes of the world, v 4.8.7. Washington, DC: Smithsonian Institution. https://doi.org/10.5479/si.GVP.VOTW4-2013
Grasso, J.-R., & Sornette, D. (1998). Testing self-organized criticality by induced seismicity. *Journal of Geophysical Research*, *103*(B12), 29965–29987. https://doi.org/10.1029/97JB01344
Gregg, P., De Silva, S., & Grosfils, E. (2013). Thermomechanics of shallow magma chamber pressurization: Implications for the assessment of ground deformation data at active volcanoes. *Earth and Planetary Science Letters*, *384*, 100–108. https://doi.org/10.1016/j.epsl.2013.09.040
Grosfils, E. (2007). Magma reservoir failure on the terrestrial planets: Assessing the importance of gravitational loading in simple elastic models. *Journal of Volcanology and Geothermal Research*, *166*(2), 47–75. https://doi.org/10.1016/j.jvolgeores.2007.06.007
Gudmundsson, A. (1984a). Formation of dykes, feeder-dykes, and the intrusion of dykes from magma chambers. *Bulletin Volcanologique*, *47*(3), 537–550. https://doi.org/10.1007/BF01961225
Gudmundsson, A. (1984b). Tectonic aspects of dykes in northwestern Iceland. *Jokull*, *34*, 81–96.
Gudmundsson, A. (1986). Formation of crystal magma chambers in Iceland. *Geology*, *14*(2), 164–166. https://doi.org/10.1130/0091-7613(1986)14%3C164:FOCMCI%3E2.0.CO;2
Gudmundsson, A. (2002). Emplacement and arrest of sheets and dykes in central volcanoes. *Journal of Volcanology and Geothermal Research*, *116*(3–4), 279–298. https://doi.org/10.1016/S0377-0273(02)00226-3
Gudmundsson, A. (2006). How local stresses control magma-chamber ruptures, dyke injections, and eruptions in composite volcanoes. *Earth-Science Reviews*, *79*(1–2), 1–31. https://doi.org/10.1016/j.earscirev.2006.06.006
Gudmundsson, A. (2011). Deflection of dykes into sills at discontinuities and magma-chamber formation. *Tectonophysics*, *500*(1–4), 50–64. https://doi.org/10.1016/j.tecto.2009.10.015
Gudmundsson, A. (2012). Magma chambers: Formation, local stresses, excess pressures, and compartments. *Journal of Volcanology and Geothermal Research*, *237*, 19–41. https://doi.org/10.1016/j.jvolgeores.2012.05.015
Gudmundsson, A. (2020). *Volcanotectonics* (1st ed.). Cambridge University Press. https://www.doi.org/10.1017/9781139176217
Hardebeck, J., Nazareth, J., & Hauksson, E. (1998). The static stress change triggering model: Constraints from two southern California aftershock sequences. *Journal of Geophysical Research*, *103*(B10), 24427–24437. https://doi.org/10.1029/98JB00573
Hardebeck, J., & Okada, T. (2018). Temporal stress changes caused by earthquakes: A review. *Journal of Geophysical Research: Solid Earth*, *123*(2), 1350–1365. https://doi.org/10.1002/2017JB014617
Hayes, G., Moore, G., Portner, D., Hearne, M., Flamme, H., Furtney, M., & Smoczyk, G. (2018). Slab2, a comprehensive subduction zone geometry model. *Science*, *362*(6410), 58–61. https://doi.org/10.1126/science.aat4723
Heap, M., Villeneuve, M., Albino, F., Farquharson, J. I., Brothelande, E., Amelung, F., et al. (2020). Towards more realistic values of elastic moduli for volcano modelling. *Journal of Volcanology and Geothermal Research*, *390*, 106684. https://doi.org/10.1016/j.jvolgeores.2019.106684

Heidbach, O., Rajabi, M., Cui, X., Fuchs, K., Müller, B., Reinecker, J., et al. (2018). The World Stress Map database release 2016: Crustal stress pattern across scales. *Tectonophysics*, *744*, 484–498. https://doi.org/10.1016/j.tecto.2018.07.007

Heuret, A., Lallemand, S., Funiciello, F., Piromallo, C., & Faccenna, C. (2011). Physical characteristics of subduction interface type seismogenic zones revisited. *Geochemistry, Geophysics, Geosystems*, *12*(1), QO1004. https://doi.org/10.1029/2010GC003230

Hildreth, W., & Moorbath, S. (1988). Crustal contributions to arc magmatism in the Andes of central Chile. *Contributions to Mineralogy and Petrology*, *98*(4), 455–489. https://doi.org/10.1007/BF00372365

Hill-Butler, C., Blackett, M., Wright, R., & Trodd, N. (2020). The co-incidence of earthquakes and volcanoes: Assessing global volcanic radiant flux responses to earthquakes in the 21st century. *Journal of Volcanology and Geothermal Research*, *393*, 106770. https://doi.org/10.1016/j.jvolgeores.2020.106770

Hill, D. P., Pollitz, F., & Newhall, C. (2002). Earthquake-volcano interactions. *Physics Today*, *55*(11), 41–47. https://doi.org/10.1063/1.1535006

Hyndman, R., Yamano, M., & Oleskevich, D. (1997). The seismogenic zone of subduction thrust faults. *Island Arc*, *6*(3), 244–260. https://doi.org/10.1111/j.1440-1738.1997.tb00175.x

Jaxybulatov, K., Shapiro, N., Koulakov, I., Mordret, A., Landès, M., & Sens-Schöenfelder, C. (2014). A large magmatic sill complex beneath the Toba caldera. *Science*, *346*(6209), 617–619. https://doi.org/10.1126/science.1258582

Kanamori, H., & Anderson, D. (1975). Theoretical basis of some empirical relations in seismology. *Bulletin of the Seismological Society of America*, *65*(5), 1073–1095.

Kanamori, H., & Kikuchi, M. (1993). The 1992 Nicaragua earthquake: A slow tsunami earthquake associated with subducted sediments. *Nature*, *361*(6414), 714–716.

Kavanagh, J., Rogers, B., Boutelier, D., & Cruden, A. (2017). Controls on sill and dyke-sill hybrid geometry and propagation in the crust: The role of fracture toughness. *Tectonophysics*, *698*, 109–120. https://doi.org/10.1016/j.tecto.2016.12.027

Kearey, P., Klepeis, K., & Vine, F. (2009). *Global tectonics* (3rd ed.). Oxford: Wiley Blackwell.

Kilb, D., Gomberg, J., & Bodin, P. (2002). Aftershock triggering by complete Coulomb stress changes. *Journal of Geophysical Research*, *107*(B4), ESE-2. https://doi.org/10.1029/2001JB000202

King, G. C. P., Stein, R. S., & Lin, J. (1994). Static stress changes and the triggering of Earthquakes. *Bulletin of the Seismological Society of America*, *84*(3), 935–953.

Kusumoto, S., Geshi, N., & Gudmundsson, A. (2013). Aspect ratios and magma overpressures of non-feeder dikes observed in the Miyake-jima volcano (Japan), and fracture toughness of its upper part. *Geophysical Research Letters*, *40*(6), 1065–1068. https://doi.org/10.1002/grl.50284

Lara, L., Lavenu, A., Cembrano, J., & Rodríguez, C. (2006). Structural controls of volcanism in transversal chains: Resheared faults and neotectonics in the Cordón Caulle-Puyehue area (40.5 S), Southern Andes. *Journal of Volcanology and Geothermal Research*, *158*(1–2), 70–86. https://doi.org/10.1016/j.jvolgeores.2006.04.017

Levandowski, W., Herrmann, R., Briggs, R., Boyd, O., & Gold, R. (2018). An updated stress map of the continental United States reveals heterogeneous intraplate stress. *Nature Geoscience*, *11*, 433–437. https://doi.org/10.1038/s41561-018-0120-x

Liao, Y., Soule, S., & Jones, M. (2018). On the mechanical effects of poroelastic crystal mush in classical magma chamber models. *Journal of Geophysical Research: Solid Earth*, *123*(11), 9376–9406. https://doi.org/10.1029/2018JB015985

Linde, A. T., & Sacks, I. (1998). Triggering of volcanic eruptions. *Nature*, *395*, 888–890. https://doi.org/10.1038/27650

Lin, J., & Stein, R. S. (2004). Stress triggering in thrust and subduction earthquakes, and stress interaction between the southern San Andreas and nearby thrust and strike-slip faults. *Journal of Geophysical Research*, *109*(B2), 1–19. https://doi.org/10.1029/2003JB002607

Lupi, M., & Miller, S. (2014). Short-lived tectonic switch mechanism for long-term pulses of volcanic activity after mega-thrust earthquakes. *Solid Earth*, *5*, 13–24. https://doi.org/10.5194/se-5-13-2014

Lupi, M., Trippanera, D., Gonzalez, D., D'amico, S., Acocella, V., Cabello, C., et al. (2020). Transient tectonic regimes imposed by megathrust earthquakes and the growth of NW-trending volcanic systems in the Southern Andes. *Tectonophysics*, *774*, 228204. https://doi.org/10.1016/j.tecto.2019.228204

Maccaferri, F., Bonafede, M., & Rivalta, E. (2010). A numerical model of dyke propagation in layered elastic media. *Geophysical Journal International*, *180*(3), 1107–1123. https://doi.org/10.1111/j.1365-246X.2009.04495.x

Maccaferri, F., Bonafede, M., & Rivalta, E. (2011). A quantitative study of the mechanisms governing dike propagation, dike arrest and sill formation. *Journal of Volcanology and Geothermal Research*, *208*(1–2), 39–50. https://doi.org/10.1016/j.jvolgeores.2011.09.001

Maccaferri, F., Rivalta, E., Keir, D., & Acocella, V. (2014). Off-rift volcanism in rift zones determined by crustal unloading. *Nature Geoscience*, *7*, 297–300. https://doi.org/10.1038/ngeo2110

Magee, C., Jackson, C.-L., & Schofield, N. (2013). The influence of normal fault geometry on igneous sill emplacement and morphology. *Geology*, *41*(4), 407–410. https://doi.org/10.1130/G33824.1

Manga, M., & Brodsky, E. E. (2006). Seismic triggering of eruptions in the far field: Volcanoes and geysers. *Annual Review of Earth and Planetary Sciences*, *34*, 263–291. https://doi.org/10.1146/annurev.earth.34.031405.125125

McGarr, A. (2014). Maximum magnitude earthquakes induced by fluid injection. *Journal of Geophysical Research: Solid Earth*, *119*(2), 1008–1019. https://doi.org/10.1002/2013JB010597

Meier, M.-A., Werner, M., Woessner, J., & Wiemer, S. (2014). A search for evidence of secondary static stress triggering during the 1992 Mw7. 3 Landers, California, earthquake sequence. *Journal of Geophysical Research: Solid Earth*, *119*(4), 3354–3370. https://doi.org/10.1002/2013JB010385

Menand, T. (2008). The mechanics and dynamics of sills in layered elastic rocks and their implications for the growth of laccoliths and other igneous complexes. *Earth and Planetary Science Letters*, *267*(1–2), 93–99. https://doi.org/10.1016/j.epsl.2007.11.043

Menand, T., Daniels, K., & Benghiat, P. (2010). Dyke propagation and sill formation in a compressive tectonic environment: Solid earth. *Journal of Geophysical Research*, *115*(B8), B08201. https://doi.org/10.1029/2009JB006791

Moore, J., & Saffer, D. (2001). Updip limit of the seismogenic zone beneath the accretionary prism of southwest Japan: An effect of diagenetic to low-grade metamorphic processes and increasing effective stress. *Geology*, *29*(2), 183–186. https://doi.org/10.1130/0091-7613(2001)029%3C0183:ULOTSZ%3E2.0.CO;2

Mpodozis, C., & Cornejo, P. (2012). Cenozoic tectonics and porphyry copper systems of the chilean andes. *Society of Economic Geologists Special Publication*, *16*, 329–360. https://doi.org/10.5382/SP.16.14

Mulargia, F., & Bizzarri, A. (2014). Anthropogenic triggering of large earthquakes. *Scientific Reports*, *4*, 6100. https://doi.org/10.1038/srep06100

Murotani, S., Satake, K., & Fujii, Y. (2013). Scaling relations of seismic moment, rupture area, average slip, and asperity size for M9 subduction-zone earthquakes. *Geophysical Research Letters*, *40*(19), 5070–5074. https://doi.org/10.1002/grl.50976

Nakamura, K. (1977). Volcanoes as possible indicators of tectonic stress orientation - principle and proposal. *Journal of Volcanology and Geothermal Research*, *2*(1), 1–16. https://doi.org/10.1016/0377-0273(77)90012-9

Nishimura, T. (2017). Triggering of volcanic eruptions by large earthquakes. *Geophysical Research Letters*, *44*(15), 7750–7756. https://doi.org/10.1002/2017GL074579

Nostro, C., Stein, R. S., Cocco, M., Belardinelli, M. E., & Marzocchi, W. (1998). Two-way coupling between Vesuvius eruptions and southern Apennine earthquakes, Italy, by elastic stress transfer. *Journal of Geophysical Research*, *103*(B10), 24487–24504. https://doi.org/10.1029/98JB00902

Okada, Y. (1992). Internal deformation due to shear and tensile faults in a half-space. *Bulletin of the Seismological Society of America*, *82*(2), 1018–1040.

Pacheco, J., Sykes, L., & Scholz, C. (1993). Nature of seismic coupling along simple plate boundaries of the subduction type: Solid earth. *Journal of Geophysical Research*, *98*(B8), 14133–14159. https://doi.org/10.1029/93JB00349

Pall, J., Zahirovic, S., Doss, S., Hassan, R., Matthews, K., Cannon, J., et al. (2018). The influence of carbonate platform interactions with subduction zone volcanism on palaeo-atmospheric CO_2 since the Devonian. *Climate of the Past*, *14*, 857–870. https://doi.org/10.5194/cp-14-857-2018

Petford, N., Kerr, R., & Lister, J. (1993). Dike transport of granitoid magmas. *Geology*, *21*(9), 845–848. https://doi.org/10.1130/0091-7613(1993)021%3C0845:DTOGM%3E2.3.CO;2

Petford, N., Cruden, A., McCaffrey, K., & Vigneresse, J.-L. (2000). Granite magma formation, transport and emplacement in the Earth's crust. *Nature*, *408*, 669–673. https://doi.org/10.1038/35047000

Piersanti, A., Spada, G., Sabadini, R., & Bonafede, M. (1995). Global post-seismic deformation. *Geophysical Journal International*, *120*(3), 544–566. https://doi.org/10.1111/j.1365-246X.1995.tb01838.x

Pinel, V., & Jaupart, C. (2005). Some consequences of volcanic edifice destruction for eruption conditions. *Journal of Volcanology and Geothermal Research*, *145*, 68–80.

Pollitz, F., Bürgmann, R., & Romanowicz, B. (1998). Viscosity of oceanic asthenosphere inferred from remote triggering of earthquakes. *Science*, *280*(5367), 1245–1249. https://doi.org/10.1126/science.280.5367.1245

Pritchard, M. E., Jay, J. A., Aron, F., Henderson, S. T., & Lara, L. E. (2013). Subsidence at southern Andes volcanoes induced by the 2010 Maule, Chile earthquake. *Nature Geoscience*, *6*, 632–636. https://doi.org/10.1038/ngeo1855

Reasenberg, P. A., & Simpson, W. (1992). Response of regional seismicity to the static stress change produced by the Loma Prieta earthquake. *Science*, *255*(5052), 1687–1690. https://doi.org/10.1126/science.255.5052.1687

Richards, J. P., Boyce, A. J., & Pringle, M. S. (2001). Geologic evolution of the Escondida area, northern Chile: A model for spatial and temporal localization of porphyry Cu mineralization. *Economic Geology*, *96*(2), 271–305. https://doi.org/10.2113/gsecongeo.96.2.271

Rikitake, T., & Sato, R. (1989). Up-squeezing of magma under tectonic stress. *Journal of Physics of the Earth*, *37*(5), 303–311. https://doi.org/10.4294/jpe1952.37.303

Rivalta, E., Taise, B., Bunger, A., & Katz, R. (2015). A review of mechanical models of dike propagation: Schools of thought, results and future directions. *Tectonophysics*, *638*, 1–42. https://doi.org/10.1016/j.tecto.2014.10.003

Rocchi, V., Sammonds, P., & Kilburn, C. (2004). Fracturing of etnean and vesuvian rocks at high temperatures and low pressures. *Journal of Volcanology and Geothermal Research*, *132*(2–3), 137–157. https://doi.org/10.1016/S0377-0273(03)00342-1

Roman, D., & Heron, P. (2007). Effect of regional tectonic setting on local fault response to episodes of volcanic activity. *Geophysical Research Letters*, *34*(13), L13310. https://doi.org/10.1029/2007GL030222

Rubin, A. (1995). Propagation of magma-filled cracks. *Annual Review of Earth and Planetary Sciences*, *23*(1), 287–336. https://doi.org/10.1146/annurev.ea.23.050195.001443

Ruprecht, P., & Plank, T. (2013). Feeding andesitic eruptions with a high-speed connection from the mantle. *Nature*, *500*(7460), 68–72. https://doi.org/10.1038/nature12342

Salfity, J. (1985). Lineamientos transversales al rumbo andino en el noroeste Argentino. In J. Frutos, R. Oyarzún, & M. Pincheira (Eds.), *Congreso geológico chileno, IV, Antofagasta, Part 2* (p. 119–137). Antofagasta: Universidad del Norte Chile.

Salfity, J., & Gorustovich, S. (1998). *The geological evolution of the province of Salta (Argentina) and neighboring regions (Tech. Rep.). Ministry of Production and Employment, Secretariat of Mining, Industry and Energy Resources*, Argentina: Salta.

Sawi, T. M., & Manga, M. (2018). Revisiting short-term earthquake triggered volcanism. *Bulletin of Volcanology*, *80*(7), 57. https://doi.org/10.1007/s00445-018-1232-2

Schellart, W., & Rawlinson, N. (2013). Global correlations between maximum magnitudes of subduction zone interface thrust earthquakes and physical parameters of subduction zones. *Physics of the Earth and Planetary Interiors*, *225*, 41–67. https://doi.org/10.1016/j.pepi.2013.10.001

Scholz, C., Tan, Y., & Albino, F. (2019). The mechanism of tidal triggering of earthquakes at mid-ocean ridges. *Nature Communications*, *10*, 2526. https://doi.org/10.1038/s41467-019-10605-2

Segall, P. (2016). Repressurization following eruption from a magma chamber with a viscoelastic aureole. *Journal of Geophysical Research: Solid Earth*, *121*(12), 8501–8522. https://doi.org/10.1002/2016JB013597

Sepúlveda, F., Lahsen, A., Bonvalot, S., Cembrano, J., Alvarado, A., & Letelier, P. (2005). Morpho-structural evolution of the Cordón Caulle geothermal region, Southern Volcanic Zone, Chile: Insights from gravity and $^{40}Ar/^{39}Ar$ dating. *Journal of Volcanology and Geothermal Research*, *148*(1–2), 165–189. https://doi.org/10.1016/j.jvolgeores.2005.03.020

Sibson, R. H. (2017). The edge of failure: critical stress overpressure states in different tectonic regimes. In J. Turner, D. Healy, R. Hillis, & M. Welch (Eds.), *Geomechanics and geology*. London: Geological Society. https://doi.org/10.1144/SP458.5

Skarlatoudis, A., Somerville, P., & Thio, H. (2016). Source-scaling relations of interface subduction earthquakes for strong ground motion and tsunami simulation. *Bulletin of the Seismological Society of America*, *106*(4), 1652–1662. https://doi.org/10.1785/0120150320

Sneddon, I., & Lowengrub, M. (1969). *Crack problems in the classical theory of elasticity*. New York, NY: Wiley.

Sparks, R. S. J., Annen, C., Blundy, J., Cashman, K. V., Rust, A., & Jackson, M. (2019). Formation and dynamics of magma reservoirs. *Philosophical Transactions of the Royal Society A*, *377*(2139), 20180019. https://doi.org/10.1098/rsta.2018.0019

Stein, R. S. (1999). The role of stress transfer in earthquake occurence. *Nature*, *402*, 605–609. https://doi.org/10.1038/45144

Strasser, F., Arango, M., & Bommer, J. (2010). Scaling of the source dimensions of interface and intraslab subduction-zone earthquakes with Moment Magnitude. *Seismological Research Letters*, *81*(6), 941–950. https://doi.org/10.1785/gssrl.81.6.941

Taisne, B., & Jaupart, C. (2009). Dike propagation through layered rocks. *Journal of Geophysical Research*, *114*(B9), B09203. https://doi.org/10.1029/2008JB006228

Tait, S., Jaupart, C., & Vergniolle, S. (1989). Pressure, gas content and eruption periodicity of a shallow, crystallising magma chamber. *Earth and Planetary Science Letters*, *92*(1), 107–123. https://doi.org/10.1016/0012-821X(89)90025-3

Tajima, R., Matsumoto, Y., & Irikura, K. (2013). Comparative study on scaling relations of source parameters for great earthquakes in inland crusts and on subducting plate-boundaries. *Zisin*, *66*(3), 31–45. https://doi.org/10.4294/zisin.66.31

Takada, Y., & Fukushima, Y. (2013). Volcanic subsidence triggered by the 2011 Tohoku earthquake in Japan. *Nature Geoscience*, *6*, 636–641. https://doi.org/10.1038/ngeo1857

Thingbaijam, K., Mai, P., & Goda, K. (2017). New empirical earthquake source-scaling laws. *Bulletin of the Seismological Society of America*, *107*(5), 2225–2246. https://doi.org/10.1785/0120170017

Tichelaar, R., & Ruff, L. (1993). Depth of seismic coupling along subduction zones. *Journal of Geophysical Research*, *98*(B2), 2017–2037. https://doi.org/10.1029/92JB02045

Toda, S., Stein, R. S., Richards-Dinger, K., & Bozkurt, S. (2005). Forecasting the evolution of seismicity in southern California: Animations built on earthquake stress transfer. *Journal of Geophysical Research*, *110*(B5), 1–17. https://doi.org/10.1029/2004JB003415

Tosdal, R. M., & Richards, J. P. (2001). Magmatic and structural controls on the development of porphyry Cu ± Mo ± Au deposits. *Reviews in Economic Geology*, *14*, 157–181. https://doi.org/10.5382/Rev.14.06

Townend, J., & Zoback, M. (2000). How faulting keeps the crust strong. *Geology*, *28*(5), 399–402. https://doi.org/10.1130/0091-7613(2000)28%3C399:HFKTCS%3E2.0.CO;2

Vrolijk, P. (1990). On the mechanical role of smectite in subduction zones. *Geology*, *18*(8), 703–707. https://doi.org/10.1130/0091-7613(1990)018%3C0703:OTMROS%3E2.3.CO;2

Walter, T. R., & Amelung, F. (2007). Volcanic eruptions following M > 9 megathrust earthquakes: Implications for the Sumatra-Andaman volcanoes. *Geology*, *35*(6), 539–542. https://doi.org/10.1130/G23429A.1

Watt, S. F. L., Pyle, D. M., & Mather, T. A. (2009). The influence of great earthquakes on volcanic eruption rate along the Chilean subduction zone. *Earth and Planetary Science Letters*, *277*(3–4), 399–407. https://doi.org/10.1016/j.epsl.2008.11.005

Wells, D., & Coppersmith, K. (1994). New empirical relationships among magnitude, rupture length, rupture width, rupture area, and surface displacement. *Bulletin of the Seismological Society of America*, *84*, 974–1002.

Ziv, A., & Rubin, A. (2000). Static stress transfer and earthquake triggering: No lower threshold in sight? *Journal of Geophysical Research*, *105*(B6), 13631–13642. https://doi.org/10.1029/2000JB900081

Ziv, A., Rubin, A., & Agnon, A. (2000). Stability of dike intrusion along preexisting fractures. *Journal of Geophysical Research*, *105*(B3), 5947–5961. https://doi.org/10.1029/1999JB900410

Zoback, M. (1992). First and second order patterns of stress in the lithosphere: The World Stress Map Project. *Journal of Geophysical Research*, *97*(B8), 11703–11728. https://doi.org/10.1029/92JB00132

Zoback, M., Zoback, M., Adams, J., Assumpção, M., Bell, S., Bergman, E., et al. (1989). Global patterns of tectonic stress. *Nature*, *341*, 291–298. https://doi.org/10.1038/341291a0